# The human genetic variant rs6190 unveils Foxc1 and Arid5a as novel pro-metabolic targets of the glucocorticoid receptor in muscle.

**Authors:** Ashok Daniel Prabakaran[1], Hyun-Jy Chung[1], Kevin McFarland[1], Thirupugal Govindarajan[1], Fadoua El Abdellaoui Soussi[1], Hima Bindu Durumutla[1], Chiara Villa[1,2], Kevin Piczer[1], Hannah Latimer[1], Cole Werbrich[1], Olukunle Akinborewa[1,3], Robert Horning[1], Mattia Quattrocelli[1,*]

**Affiliations:**

[1] Molecular Cardiovascular Biology, Heart Institute, Cincinnati Children's Hospital Medical Center and Dept. Pediatrics, University of Cincinnati College of Medicine, Cincinnati, OH, USA;

[2] Stem Cell Laboratory, Department of Pathophysiology and Transplantation, Dino Ferrari Centre, University of Milan, Italy;

[3] Systems Biology and Physiology Graduate Program, University of Cincinnati College of Medicine, Cincinnati, OH 45229, USA.

*** Corresponding Author:**

Mattia Quattrocelli, PhD, Molecular Cardiovascular Biology, Heart Institute, Cincinnati Children's Hospital Medical Center, 240 Albert Sabin Way T4.676, Cincinnati, OH 45229. Email: mattia.quattrocelli@cchmc.org, tel: +1-513-517-1221.

**Keywords** - Glucocorticoid receptor, rs6190, muscle metabolism, insulin sensitivity, glucose tolerance, fatty acid uptake.

**Data availability** - RNA-seq and ChIP-seq datasets reported here are available on GEO as entries GSE262234 and GSE262235.

**Conflicts of interest** – All Authors declare no competing interests.

## Abstract

Genetic variations in the glucocorticoid receptor (GR) gene *NR3C1* can impact metabolism. The single nucleotide polymorphism (SNP) rs6190 (p.R23K) has been associated in humans with enhanced metabolic health, but the SNP mechanism of action remains completely unknown. We generated a transgenic knock-in mice genocopying this polymorphism to elucidate how the mutant GR impacts metabolism. Compared to non-mutant littermates, mutant mice showed increased muscle insulin sensitivity and strength on regular chow and high-fat diet, blunting the diet-induced adverse effects on weight gain and exercise intolerance. Overlay of RNA-seq and ChIP-seq profiling in skeletal muscle revealed increased transactivation of *Foxc1* and *Arid5A* genes by the mutant GR. Using adeno-associated viruses for in vivo overexpression in muscle, we found that *Foxc1* was sufficient to transcriptionally activate the insulin response pathway genes *Insr* and *Irs1*. In parallel, *Arid5a* was sufficient to transcriptionally repress the lipid uptake genes *Cd36* and *Fabp4*, reducing muscle triacylglycerol accumulation. Collectively, our findings identify a muscle-autonomous epigenetic mechanism of action for the rs6190 SNP effect on metabolic homeostasis, while leveraging a human nuclear receptor coding variant to unveil *Foxc1* and *Arid5a* as novel epigenetic regulators of muscle metabolism.


## Graphical abstract

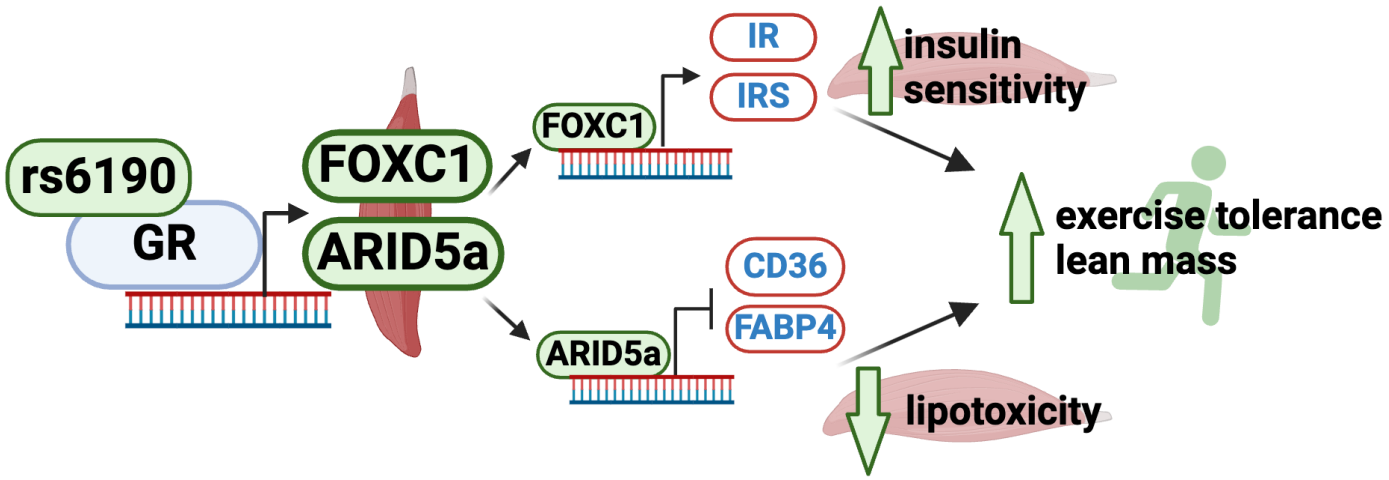

## Introduction

Insulin resistance is a well-known pathophysiological marker and risk factor for type 2 diabetes and cardiovascular diseases arbitrated by altered insulin signaling pathway [1]. Indeed, the insulin resistance observed in obese diabetic subjects directly impacts metabolic health through reduced systemic glucose clearance and progressive loss of lean muscle mass [2; 3]. Recent successes in glycemic control through antihyperglycemic drugs are positively impacting the management heart failure risk [4; 5]. However, muscle-centered mechanisms to rescue lean mass and strength in conditions of insulin resistance remain very limitedly elucidated. This becomes critical considering the sharp rise in prevalence of diabetes and obesity among adults, which will near about 50% of the global population by 2040 [6; 7] and therefore create an urgent need to identify molecular targets that could remodel the insulin resistant muscle towards metabolic competence. Indeed, skeletal muscle is a major determinant (up to 80%) of insulin-mediated glucose disposal and utilization in both humans and rodents [8; 9].

Glucocorticoids (GC) exert multiple pleotropic actions critical for metabolic, physiological, and stress-related conditions through activation of the glucocorticoid receptor (GR; *NR3C1* gene) [10; 11]. Glucocorticoids (GCs) play a crucial role in regulating metabolic homeostasis of glucose, lipid and protein in skeletal muscle development [12-14]. The response of skeletal muscle to the GR action is modulated by single nucleotide polymorphisms (SNPs) that can impact metabolic homeostasis through a modified GR protein function [15]. In humans, several SNPs within the 9 exons of the GR gene have been identified and studied for their association with glucocorticoid sensitivity and pathophysiological impact on human health [16; 17]. These genetic variations can affect the function, expression, or regulation of the glucocorticoid receptor, leading to differences in the individual response to glucocorticoid hormones [18]. Intriguingly, some single nucleotide polymorphisms (SNPs) including Asn363Ser (rs6195) and BclI (rs41423247) are associated with enhanced exogenous and endogenous glucocorticoid sensitivity predisposing those carriers to metabolic dysfunction that includes increased BMI, low bone density, insulin resistance and altered cholesterol levels that promote cardiovascular risk [19; 20] . On the contrary, the rs6190 SNP (p. R23K; also known as ER22/23EK because in complete linkage with the silent E22E rs6189 SNP) correlated with enhanced muscle strength, lean body mass and metabolic health in men in limited human cohorts [21-23]. However, genetic proof and mechanism of action for a direct effect of rs6190 on metabolic health are still missing.

To investigate the mechanism of this variant GR we generated transgenic mice genocopying the rs6190 SNP to test whether and how the SNP affects metabolism. Based on transcriptomic and epigenomic datasets from muscle, we further explored Forkhead box C1 (*Foxc1* gene) and AT-Rich Interaction Domain 5A (*Arid5A* gene) as novel muscle-autonomous transactivation targets responsible for the mutant GR action on metabolism and action. Further, we validated requirement and sufficiency for these two factors in insulin sensitivity and muscle lipid accumulation through AAV-based myocyte-specific overexpression. We further probed the large UK Biobank dataset to query for the SNP effect on markers of glucose homeostasis and strength. Our study leverages a human SNP mechanism of action to identify novel myocyte-autonomous targets to salvage exercise tolerance and lean mass from metabolic stress.

## Results

*$GR^{R24K/R24K}$ mice exhibit improved exercise tolerance and glucose homeostasis.*

In order to gain direct genetic and biological insight in understanding the role of the non-synonymous coding rs6190 SNP in the GR gene *NR3C1* (transcript ENST00000231509.3 (- strand); c.68G>A; p.R23K)[24], we generated a transgenic mouse model where we CRISPR-knocked-in a single nucleotide mutation in the orthologous codon of the endogenous murine *Nr3c1* gene (NM_008173 transcript; c.71G>A, p.R24K; **Fig. 1A**). We then compared homozygous mutant mice ($GR^{R24K/R24K}$) to non-mutant littermates ($GR^{wt/wt}$) to maximize the potential SNP effect and simplify the comparison through homogenous GR pools (100% mutant vs 100% non-mutant GR pools). Also, we focused our comparisons on young adult (4mo) male mice considering the seminal correlations of the SNP with metabolic health in young adult men [25].

We first compared growth and body composition. $GR^{R24K/R24K}$ mice showed a smaller but leaner body compared to $GR^{wt/wt}$ littermates at 4 months of age, i.e. smaller weight with lower fat mass contribution and higher lean mass contribution **(Figure 1B)**. We tested for exercise tolerance through treadmill exercise, grip strength and muscle force (in vivo hindlimb dorsiflexion assay [26]). Compared to $GR^{wt/wt}$, $GR^{R24K/R24K}$ mice exhibited increased values of treadmill work until exhaustion, bilateral forelimb grip strength normalized to body mass and max hindlimb dorsiflexion force **(Figure 1B)**. We then tested the overall glucose homeostasis through fasting glycemia, fed-state glycemia and HOMA-IR values [27], as well as glucose tolerance, insulin tolerance and muscle 2DG uptake assays [28]. Compared to $GR^{wt/wt}$, $GR^{R24K/R24K}$ mice showed decreased glycemia either in fasting or fed states, decreased HOMA-IR and, consistently, improved glucose/insulin tolerance curve profiles and increased 2DG uptake in muscle **(Figure1C)**. Considering the apparent increase in muscle insulin sensitivity, we further characterized muscles for myofiber typing, myofiber cross-sectional area and oxidative function. Compared to $GR^{wt/wt}$, $GR^{R24K/R24K}$ mice showed a partial shift in mixed-fiber muscles towards oxidative fibers, as shown by immunostaining, WBs and qPCRs for Myh4 (type 2B), Myh2 (type 2A) and Myh7 (type 1) **(Figure 1D)**. Compared to $GR^{wt/wt}$, $GR^{R24K/R24K}$ muscle showed increased myofiber cross-sectional area, a parameter indicative of gained muscle mass **(Figure 1E)**. We also tested muscle glucose oxidation, a direct marker of muscle insulin sensitivity [29]. Glucose oxidation in muscle tissue was increased in $GR^{R24K/R24K}$ muscle, as shown by basal respiration and calculated ATP production in glucose-fueled Seahorse assays using muscle tissue biopsies[30] **(Figure 1F)**. The gain in respiration was paralleled by an increase in mitochondrial complex WB signal **(Figure 1F)**. Collectively, these findings indicate that the rs6190 SNP can directly impact exercise tolerance, glucose homeostasis and lean mass in experimental conditions of genetic background homogeneity.

*In muscle, the mutant GR exhibits a specific transactivation program targeting Foxc1 and Arid5a.*

Because the amino acid substitution R24K is in the N-terminal domain of the GR, which mediates protein-protein interactions [31], we sought to gain insight in potential changes in the GR interactions with other proteins in vivo. We performed an immunoprecipitation-mass spectrometry screening for GR interacting proteins in quadriceps muscles of $GR^{wt/wt}$ (100% WT GR) vs $GR^{R24K/R24K}$ (100% mutant GR) male mice. Strikingly, we found that the

124 mutant GR displayed a strong downregulation in binding of Hsp70 **(Figure 2A)**. Because Hsp70 is a major
125 cytoplasmic docker for the GR before its nuclear translocation [32], we tested the mutant GR translocation
126 capacity in muscle comparing the GR protein signal in nuclear vs cytoplasmic fractions at 30min after a single
127 dexamethasone injection. Compared to the WT GR, the mutant GR showed increased nuclear translocation
128 capacity **(Figure 2B)**. Considering the skew in nuclear translocation, we tested the extent to which the SNP
129 changed the epigenomic activity of the muscle GR through muscle GR ChIP-seq in quadriceps muscle. The GR
130 binding element (GRE) motif was the top enriched motif in the datasets from both $GR^{wt/wt}$ and $GR^{R24K/R24K}$
131 muscles, as well as the typical expected GR peaks on the canonical GR reporter *Fkbp5* promoter were clearly
132 defined **(Figure 2C)**, validating our datasets. Genome-wide occupancy on GRE motifs was increased by the
133 mutant GR, as shown by density plot and heatmaps, although no genotype-related shifts in overall peak
134 distribution (highly enriched in promoter-TSS regions) were observed **(Figure 2D)**. To find potential gene targets
135 of the increased epigenomic activity of the mutant GR, we overlayed our ChIP-seq datasets with RNA-seq
136 datasets that were obtained from subfractions of the same muscle samples. We ranked differentially expressed
137 genes for mutant GR-dependent gains in GR peak signal in the promoter-TSS region and in overall RNA fold
138 change, and we *found forkhead box C1* (*Foxc1* gene) and *AT-Rich Interaction Domain 5A (Arid5A* gene) as top
139 hits **(Figure 2D)**. Indeed, both genes show a clear gain of promoter-TSS GR peak in $GR^{R24K/R24K}$ muscles **(Figure**
140 **2E)**. Taken together, these data show that in muscle the SNP increases the epigenetic GR activity that fuels
141 transactivation of a specific gene program involving *Foxc1* and *Arid5a*.

142

143 *Foxc1 promotes Insr/Irs1 expression and muscle insulin sensitivity*

144 Foxc1 is a Forkhead-box transcription factor implicated in Axenfeld-Rieger syndrome[33] and kidney
145 development [34], but <u>never studied in muscle and metabolism.</u> Cross-check through the predictive tool
146 Harmonizome [35] unveiled that *Insr* (insulin receptor) and *Irs1* (insulin receptor substrate 1) genes were putative
147 targets of *Foxc1* and were indeed the top upregulated genes in the enriched "insulin/IGF pathway" gene ontology
148 term per $GR^{R24K/R24K}$ vs $GR^{wt/wt}$ RNA-seq comparison **(Figure 3A)**. *Insr* and *Irs1* showed increased *Foxc1* binding
149 on canonical F-box sites on their promoters in $GR^{R24K/R24K}$ vs $GR^{wt/wt}$ muscle in subsequent ChIP-qPCR
150 validations **(Figure 3B)**. Accordingly in the mutant muscle, upregulated FOXC1 protein levels correlated with
151 increased INSR and IRS1 total levels, decreased inhibitory phosphorylation on IRS1 Ser307 (marker of IRS1
152 degradation in insulin resistant muscle [36]) and increased activating phosphorylation on AKT Ser473 (marker
153 of insulin responsiveness [37]) **(Figure 3C)**. In vitro, *Foxc1* overexpression through C2C12 myoblast transfection
154 increased the total protein levels of INSR and IRS1, activating insulin-stimulated 2DG uptake in myotubes
155 **(Figure 3D).** To test *Foxc1* sufficiency in muscle in vivo, we generated AAVs to overexpress either GFP (control)
156 or *Foxc1* downstream of a *CMV* promoter. A strong adult myocyte tropism was promoted by using the MyoAAV
157 serotype [38]. At 2 weeks after a single r.o. injection of $10^{12}$vg/mouse in WT mice, we found that *Foxc1*
158 overexpression increased Insr and Irs1 levels, as well as muscle 2DG uptake **(Figure 3E)**. Taken together, these
159 data indicate that the *Foxc1* transactivation by the mutant GR in muscle is sufficient to promote the gain in insulin
160 pathway gene expression, unveiling *Foxc1* as unanticipated regulator of muscle insulin sensitivity.

*Arid5A represses CD36 and FABP4 expression and lowers triacylglycerol content in muscle*

*Arid5A* has been reported in adipose tissue as pro-metabolic factor by repression of lipid transport genes *Cd36* and *Fabp4* expression [39], but its function in muscle remains virtually unknown. Compared to $GR^{wt/wt}$, the *Arid5A* upregulation in $GR^{R24K/R24K}$ muscle correlated with downregulation of *Cd36* and *Fabp4* levels, which in turn showed increased occupancy of Arid5A on their gene promoter sites **(Figure 4A)**. In silico prediction through STRING [40] suggested possible interaction of Arid5A with the repressor SAP30, a component of the repressive histone deacetylation complex that includes HDAC1 and SIN3A [41]. Considering the apparent increase in levels and repressive activity by Arid5a in the mutant muscle, we tested these protein interactors through CoIP and found that the mutant muscle showed increased recruitment of SAP30, HDAC1 and SIN3A proteins by Arid5A **(Figure 4B)**. In line with the reported role of *Arid5a* in limiting lipid uptake and storage in adipose tissue [39], compared to $GR^{wt/wt}$ the $GR^{R24K/R24K}$ muscle showed lower levels of muscle triacylglycerol accumulation **(Figure 4C)**. We confirmed *Arid5A* genetic sufficiency for downregulation of CD36 and FABP4 expression as well as triacylglycerol content in muscle through in vitro (C2C12 myoblast transfection) and in vivo (AAV transduction) assays **(Figure 4D-E)**. Taken together, these data support that the *Arid5A* transactivation by the mutant GR in muscle is sufficient to decrease muscle triacylglycerols, unveiling *Arid5A* as novel regulator of muscle lipid accumulation.

*The mutant GR protects form diet-induced metabolic stress*

Considering the transcriptional and metabolic effects of the mutant GR in muscle in conditions of regular chow, we sought to quantitate the extent to which the apparent pro-metabolic program enabled by the SNP withstood the challenge of high-fat diet-induced metabolic stress. We exposed $GR^{wt/wt}$ and $GR^{R24K/R24K}$ littermates to 12-week-long ad libitum feeding with high-fat (60% kcal) diet. At endpoint and compared to $GR^{wt/wt}$, $GR^{R24K/R24K}$ mice showed reduced body weight accrual and fat mass, with increased lean and muscle mass **(Figure 5A)**. Mutant obese mice showed increased values of running endurance on the treadmill, grip strength and hindlimb force compared to control obese littermates **(Figure 5B)**. Also at endpoint, mutant obese mice showed reduced values of fasted- and fed-state glycemia, HOMA-IR, glucose intolerance and increased trends of insulin tolerance and muscle 2DG glucose uptake **(Figure 5C)**. We then quantitated the *Foxc1* and *Arid5a* cascades in the muscles of obese $GR^{wt/wt}$ versus $GR^{R24K/R24K}$ mice. Analogously to what we previously found in regular chow conditions, *Foxc1* and the insulin response pathway appeared upregulated and activated **(Figure 5D)**, as well as *Arid5A* repressive action on *Cd36*, *Fabp4* **(Figure 5E)**. Finally, we tested the extent to which the concerted increase in *Foxc1* and *Arid5a* in muscle was sufficient to mimic the SNP metabolic protective effect with high-fat diet. We injected WT mice with the combination of MyoAAV-Foxc1 and MyoAAV-Arid5a, using the control vector (GFP) as control, and then exposed them to the same 12-week-long high-fat diet. Overexpression of both factors in muscle recapitulated the molecular effects of each factor (Insr and Irs1 gain for Foxc1; Cd36 and Fabp4 loss for Arid5A) and resulted in improved glucose homeostasis and muscle lipid accumulation, as shown by reduced

197 fasting glycemia, increased muscle 2DG uptake and reduced muscle triacylglycerols **(Figure 5F)**. Taken
198 together, these data indicate that the myocyte-autonomous Foxc1-Arid5a program enabled by the mutant GR is
199 sufficient to improve exercise tolerance and insulin sensitivity in conditions of diet-induced metabolic stress.

200

201 *Data from the UK Biobank support a pro-metabolic effect of the mutant GR in humans*

202 To gain further insight in the relevance of our SNP-related findings for humans, we probed the large dataset of
203 the UK Biobank that comprises data from 485,895 adults of ~40-70 years of age. In this cohort, the GR rs6190
204 variant (NR3C1 gene, transcript ENST00000231509.3 (- strand); c.68G>A; p.R23K) exhibited a minor allele
205 frequency of 2.68%, with 25,944 heterozygous individuals and 413 homozygous individuals for the rs6190 SNP.
206 We focused on parameters of relevance aligned with our prior measures of metabolic and muscle function, i.e.
207 glycemia, body mass index (BMI), lean mass and hand grip strength normalized to arm lean mass. Consistent
208 with prior associations in men [25], we also found significant associations of rs6190 SNP in the male UK Biobank
209 population with BMI, glycemia and hand grip strength through regression analysis with age as co-variate **(Table**
210 **1)**. In line with our $GR^{wt/wt}$ versus $GR^{R24K/R24K}$ comparisons in mice, we compared homozygous male carriers of
211 the alternative rs6190 SNP allele (ALT/ALT) to homozygous male carriers of the reference allele (REF/REF) in
212 cross-sectional comparisons of median values per parameter. In the absence of changes in age, ALT/ALT
213 individuals showed reduced median levels of glycemia and BMI and increased median levels of lean mass and
214 grip strength when compared to REF/REF individuals **(Figure 6A)**. It must be noted that these trends are still
215 significant for glycemia and BMI and almost significant for lean mass and grip strength when the values from
216 heterozygous individuals are included in three-groups comparisons **(Table 2)**. Together with our genetic studies
217 in mice, these data further support the potential relevance of the pro-metabolic mechanisms enabled by the
218 rs6190-mutant GR for human health.

219

**Table 1. Regression analyses for rs6190 vs hand grip strength (HGS), BMI and glycemia in the UK Biobank male population.**

| | Estimate | Std. Error | t value | Pr(>\|t\|) | |
|---|---|---|---|---|---|
| Hand grip strength/lean arm mass | 0.0297597 | 0.0018382 | 16.19 | <2e-16 | *** |
| BMI | -0.0169335 | 0.0011282 | -15.009 | <2e-16 | *** |
| Glycemia | -0.0691419 | 0.0031062 | -22.26 | <2e-16 | *** |
| covariates: age | | | | | |
| Signif. codes: 0 '***' 0.001 '**' 0.01 '*' 0.05 '.' 0.1 ' ' 1 | | | | | |
| | | | | | |
| Residual standard error: 0.8805 on 45101 degrees of freedom | | | | | |
| (165529 observations deleted due to missingness) | | | | | |
| Multiple R-squared: 0.04511, | | | | | |
| F-statistic: 355.1 on 6 and 45101 DF, p-value: < 2.2e-16 | | | | | |

**Table 2. Comparisons for each parameter between homozygous individuals for the reference allele, heterozygous and homozygous for the rs6190 alternative allele in the UK Biobank male population.**

| Parameter, N | REF | HET | P-value vs REF | HOMO | P-value vs REF |
|---|---|---|---|---|---|
| Age in years | 58 (58 – 58) | 58 (58 – 59) | 0.1638 | 58 (56 – 59) | >0.9999 |
| N | 210446 | 11811 | | 191 | |
| Glycemia in mM | 4.956 (4.953 – 4.959) | 4.926 (4.915 - 4.937) | **<0.0001** | 4.881 (4.793 - 4.980) | **0.0218** |
| N | 183988 | 9657 | | 159 | |
| BMI in kg/m$^2$ | 27.30 (27.28 - 27.32) | 27.29 (27.21 - 27.38) | **0.0517** | 26.95 (25.99 - 27.71) | **0.0469** |
| N | 209459 | 11556 | | 178 | |
| Hand grip strength/lean arm mass in kg/kg | 11.58 (11.56 - 11.58) | 11.56 (11.50 - 11.61) | 0.9477 | 11.95 (11.37 - 12.35) | **0.0636** |
| N | 205953 | 11544 | | 178 | |
| Lean mass in % of body mass | 74.64 (74.61 - 74.66) | 74.61 (74.46 - 74.73) | >0.9999 | 75.85 (74.66 - 76.77) | **0.0622** |
| N | 206356 | 11582 | | 184 | |

Values are presented as median (95% CI); Kruskal-Wallis test with Dunn's multiple comparison. P-values lower or close to 0.05 were highlighted in bold.

228 **Discussion**

229 Muscle insulin sensitivity is critical for metabolic health [8], as skeletal muscle accounts for ~80% of glucose
230 uptake postprandial [42] or after an oral bolus [43]. The insulin-resistant muscle progressively loses mass and
231 function, exacerbating the vicious circle of metabolic stress and exercise intolerance [44]. Indeed, in type-2
232 diabetes, muscle insulin resistance generally precedes beta cell failure and overt hyperglycemia [45]. <u>However,
233 the quest for actionable muscle-autonomous mechanisms to rescue insulin sensitivity is still open.</u> Here we
234 leverage the mechanism of action of the rs6190-mutant GR in muscle to unveil the potentially critical role of
235 Foxc1 and Arid5a as muscle-autonomous factors sufficient to promote overall insulin sensitivity and reduce
236 lipotoxicity. Albeit their genetic requirement is still yet to be rigorously tested, our in vivo sufficiency proof through
237 AAV-driven overexpression indicate a significant effect for their gain-of-function on glucose homeostasis and
238 resistance to metabolic stress, particularly in the context of high-fat diet. It must also be noted that our study is
239 the first to report myocyte-autonomous roles and molecular targets for both Foxc1 and Arid5a in muscle, paving
240 the way to future studies delving in those cascades.

241 Glucocorticoid steroids and the glucocorticoid receptor (GR) constitute a primal circadian axis regulating glucose
242 homeostasis and insulin sensitivity, as evidenced by the prefix "gluco" and the long-known effects on liver
243 gluconeogenesis[46] and adipose tissue lipolysis[47]. Glucocorticoids are widely prescribed to manage
244 inflammation and are used by over 2.5mln people for over 4 years in the US alone [48]. Typically, glucocorticoids
245 are prescribed to be taken once-daily at the start of our active-phase (early morning) [49], but such glucocorticoid
246 regimens are very well known to disrupt insulin sensitivity, particularly in muscle [12]. Recently, we have
247 discovered that intermittence in chronic frequency-of-intake [50] and early rest-phase as circadian time-of-intake
248 [51] uncover pro-ergogenic glucocorticoid-GR mechanisms in muscle. In that regard, GR mechanisms of insulin
249 sensitization are emerging in non-muscle cells, from the adipocyte GR stimulating adiponectin [50] to the
250 macrophage GR protecting against insulin resistance [52]. <u>However, myocyte-autonomous mechanisms of
251 insulin sensitization by the glucocorticoid receptor remain quite unanticipated in the field.</u> Here we report that a
252 non-synonymous human variant in the glucocorticoid receptor skews its activity towards a pro-metabolic program
253 in muscle. Our muscle-centered study is the first in vivo investigation of the potential physiologic mechanisms
254 enabled by the rs6190-mutant GR, and future studies in other tissues of metabolic interest will help articulate an
255 holistic paradigm for the metabolic impact of this non-rare mutant GR in the human population.

256 We are focusing on Foxc1 and Arid5A as putative muscle GR effectors of insulin sensitivity and lipotoxicity
257 protection thanks to a rather uncommon angle, i.e. the human GR variant rs6190. Traditionally, rs6190 is referred
258 to as ER22/23EK or rs6189/rs6190 due to the complete linkage with the silent rs6189 SNP on the previous
259 codon (E->E). The rs6190 SNP case is fascinating because a theoretically inconsequential coding variant
260 (conservative replacement R->K in position 23) associated with lower levels of fasting insulin and HOMA-IR [22],
261 increased lean mass and muscle strength as young adults [25], and prolonged survival as older adults [53]. The
262 proposed mechanism of "glucocorticoid resistance", based on limited in vitro observations [54], was largely
263 unreproducible in many other association studies [24; 55-60]. <u>Thus, the extent to which the coding rs6190 GR
264 variant is sufficient to directly regulate insulin sensitivity, as well as the underlying mechanism, remain unknown.</u>

We re-assessed the rs6190 associations in the large UK Biobank dataset, and tested sufficiency and mechanism for the SNP in CRISPR-engineered mice, confirming that the SNP is sufficient to increase muscle insulin sensitivity. However, in contrast to previously proposed “glucocorticoid resistance”, we found that in muscle tissue the SNP increased the dexamethasone-induced nuclear translocation (GR activation), as well as its epigenomic activity. Also, we found Foxc1 and Arid5A as mutant GR-specific targets of transactivation in muscle. Therefore, taken together, our data challenge the paradigm of this mutation on GR activity at least in muscle, and open a compelling avenue of investigation in other systems of relevance, like liver, adipose tissue and immune system.

**Acknowledgements -** Mass-spec analyses were performed thanks to the Proteomics Mass-Spec Core Facility at University of Cincinnati, with critical assistance by Dr. Greis and Dr. Haffey. Next-generation sequencing was performed thanks to the Cincinnati Children’s DNA Sequencing and Genotyping Facility (RRID: SCR_022630), with critical assistance by David Fletcher, Keely Icardi, Julia Flynn, and Taliesin Lenhart.

**Grant support –** This work was supported by R01HL166356-01, R03DK130908-01A1, R01AG078174-01 (NIH) and RIP, CCRF Endowed Scholarship, HI Translational Funds (CCHMC) grants to MQ.

## Material and Methods

### Mice handling and Transgenic mice generation

Mice handling and maintenance in polypropylene cages with chow diet and water ad libitum were done as per the American Veterinary Medical Association (AVMA) and under protocols fully approved by the Institutional Animal Care and Use Committee (IACUC) at Cincinnati Children's Hospital Medical Center (#2022-0020, #2023-0002). Mice, which is a well-established model system for metabolic research were maintained in a controlled room temperature of @22°C with 14/10 hr light/dark cycle in a purpose build pathogen free animal facility consistent with the ethical approval. Periodic change of cages, with fresh water and beds, was done to ensure a healthy and stress-free environment for the animals. Rodent diet with 60 kcal% fat (Research Diets, D12492) was used to generate High Fat Diet induced obese (HFD) animal groups.

WT mice were obtained and interbred from the Jakson Laboratories (Bar Harbor, ME; JAX strain) as WT C57BL/6 mice #000664. Transgenic mice genocopying the polymorphism R24K was established through the CRISPR/Cas9 genome editing in the endogenous *Nr3c1* locus on the C57BL/6J background. This genetic modification was performed by the Transgenic Animal and Genome Editing Core Facility at CCHMC. To ensure genetic background homogeneity and control for potential confounding variables, the colonies were maintained through heterozygous mattings. This approach allowed us to compare two distinct groups of male mice as littermates: $GR^{wt/wt}$ (control WT) and $GR^{R24K/R24K}$ (homozygous SNP carriers) in homogenous genetic background conditions.

### DNA isolation and Genotyping

DNA isolation from tail/ muscle tissue for genotyping experiments were done using the kit from G biosciences (#786-136). Briefly, Samples (ear, toe, tail and muscle tissue) were collected in a 1.5ml micro centrifuge tube containing 500ul of genomic lysis buffer and 10ul of proteinase K solution incubated on thermomixer at 60C for 3-4 hrs or overnight. The samples were cooled to room temperature and 200ul of chloroform were added and mixed by inverting several times centrifuged at 14000g for 10 minutes. The upper phase was separated to a new clean 1.5 ml micro centrifuge tube and 150ul of precipitation solution were added and centrifuged for 5 min at 14000g. Transfer the supernatant to a new 1.5 ml micro centrifuge tube and add 500ul isopropanol invert it several times and centrifuge at 14000g for 5 min to precipitate the genomic DNA. Add 700ul of 70% ethanol to wash the DNA pellet and centrifuge for 1min at 14000g. decant the ethanol and air dry the pellet for 5 min or until no ethanol is observed. Add 50ul of MilliQ water to the DNA pellet and incubate in the thermomixer at 55C for 15 min to rehydrate or at 4C in fridge O/N.

Genotyping the R24K mice carrying the $GR^{wt/wt}$ / $GR^{R24K/R24k}$ polymorphism were genotyped by PCR-RFLP method. Briefly, 18 µl of PCR master mix which includes MM (Promega #xxx), 1ul of Forward/Reverse primers (10mM), nuclease free water and 2 µl of the isolated DNA were subjected to Polymerase chain reaction with the 40 cycles (95C-10 min and 40 cycle of 95C-30sec, 55C-30sec, 72C-30sec and final 72C- 5min). After the PCR 20ul of the PCR product were restriction digested with BamH1 (NEB #xxx) for 1 hr at 37C. The digested PCR

320 product was resolved on 2% Agarose gel and visualized in a UV transilluminator. The mice genotypes were
321 denoted based on their band size ($GR^{wt/wt}$- xbp and $GR^{R24K/R24K}$- xbp). Primers used for the genotyping; For-
322 TGTACATTTAGCGAGTGGCAGGAT; Rev- TGCTGAGCCTTTTGAAAAATCAAG; GR wild type has a band size
323 of 474bp while the GR R24K -14bp.

324 **Tissue and blood collection, assessment of glucose and insulin tolerance test and 2-DG uptake,**
325 **Triglyceride estimation**

326 All young adult mice (4-month-old) used for the experiments were euthanized through carbon dioxide inhalation
327 followed by cervical dislocation and tissues of metabolic relevance such as skeletal muscle (soleus and
328 gastrocnemius) was dissected out using a sterile surgical kit, rapidly snap frozen in liquid nitrogen and stored at
329 -80°C for further analysis.

330 Blood collections were carried out by tail snip or euthanasia method. For the tail snip method, pups or the rats
331 were restrained in the cage with the lid closed having the tail outside, and one or 2 mm of the tail tip was quickly
332 cut using sterilized surgical scissors. By gently squeezing the tail from the base, the blood was collected and
333 assessed for hyperglycemia using a glucometer (OneTouch® Ultra® 2 meter). For serum collection, the animals
334 were euthanized, and around 1 to 2 ml of blood withdrawn using a sterile syringe from the abdominal aorta
335 (unlock 3 ml syringe,). The blood was allowed to stand at room temperature, centrifuged at 5000 rpm for 5 min
336 and the serum was transferred to a new tube and stored at -80°C for further analysis.

337 To perform glucose tolerance test on mice fed on standard chow and HFD diet, were fasted for overnight (12-
338 16hrs). The fasting glucose levels were assessed by tail snip method as described above using a glucometer as
339 described. After the fasting glucose assessment, an intraperitoneal injection of D-glucose solution (Sigma,
340 G8270) was injected at a rate of 2 g/kg body weight concentration to all the groups. The blood glucose levels
341 were assessed by tail snip method at every 30 min till 2 hours post glucose injection and recorded. mice were
342 then sacrificed, and the tissues and serum samples were collected as above. The same procedure was followed
343 for insulin tolerance test with the fasted mice after glucose measurement at baseline injected with 0.5U/Kg insulin
344 in 100ul PBS. Glycemia was recorded every 30 min post injection. The HOMA-IR calculation for analyzing the
345 insulin resistance was also undertaken[61].

346 The 2-DG glucose uptake for tissues was analyzed by Promega Glucose uptake -Glo assay method (#J1341).
347 Briefly, 1mM solution of 2DG was injected into the mice 30 min before euthanasia. Tissue such as skeletal
348 muscle was collected and crushed into fine powder and 20-50mg was used for the assay. Thaw all the reagents
349 at room temperature and mix 25ul of neutralization buffer to 100ul of the reaction mixture per reaction to the
350 powdered tissue. Mix and let it sit for 0.5- 5 hours and centrifuge of 5 min at 10000g. Separate 125µl of the
351 supernatant into 96 well plate and read luminescence on a plate reader. In the same way the triglyceride
352 accumulation and insulin were quantitated by kit method as per manufacturer's protocol (CYMAN chemical #
353 10010303; 589501).

354 **RNA isolation, RNA- Sequencing, cDNA synthesis and Qualitative PCR analysis**

RNA isolation was carried out by the standard Trizol method [62]. The tissue sample was cut into pieces using a sterile blade and transferred to a 2 ml Eppendorf tube to which 1ml of Trizol reagent (Invitrogen # 15596018) was added. The tissue was homogenized using a Tissue lyzer (Benchmark, D1000) and 0.2 ml of chloroform was added and vortexed. The sample was centrifuged at 14000 rpm for 15 min which formed 3 different layers. The upper aqueous layer which contains the RNA, is separated into a new 1.5 ml Eppendorf tube and 500 µl of isopropyl alcohol was added, mixed by inverting and centrifuged at 14000 rpm for 10 min. After centrifugation, the pellet was washed with 70% ethanol and centrifuged at 14000 rpm for 10 min. Purification of RNA was carried out by adding 200 µl of DNase 1 buffer containing 5 µl of DNase 1. The pellet was reconstituted and incubated at 370C for 30 min. After incubation, 200 µl of lysis buffer and 200 µl of MPC solution was added, vortexed and incubated in ice for 5 min. Following incubation, the mixture was vortexed and centrifuged at 14000 rpm for 10 min. This step precipitates the proteins and salts leaving the upper aqueous layer containing the RNA which was separated carefully into a new tube and 500 µl of isopropanol were added and the tube was inverted several times and centrifuged at 14000 rpm for 10min to pellet the RNA. The pellet was washed using 70% ethanol by adding 500ul to the tube and centrifuged at 14000 rpm for 10 min. The tube was air-dried at room temperature and the pelleted RNA was re-suspended with 30 µl of milliQ water.

RNA-seq was performed at the DNA Core at the CCHMC facility with 10 ng – 150 ng of total RNA used after quantification by Qubit RNA HS assay kit (Cat #Q32852; Invitrogen, Waltham, MA). Based RNA integrity value above 7 determined by the spectrofluorometric measurement RNA samples was poly-A selected and reverse transcribed using Illumina's TruSeq stranded mRNA library preparation kit (Cat# 20020595; Illumina, San Diego, CA). Library preparation was done for each sample fitted with one of 96 adapters with different 8 base molecular barcode for high level multiplexing and following 15 cycles of PCR amplification, completed libraries were sequenced on an Illumina NovaSeqTM 6000, generating 20 million or more high quality 100 base long paired end reads per sample. A quality control check on the fastq files was performed using Fast QC. Upon passing basic quality metrics, the reads were trimmed to remove adapters and low-quality reads using default parameters in Trimmomatic [Version 0.33]. In the next step, transcript/gene abundance was determined using kallisto [Version 0.43.1]. The trimmed reads were then mapped to mm10 reference genome using default parameters with strandness (R for single-end and RF for paired-end) option in Hisat2 [Version 2.0.5]. In the next step, transcript/gene abundance was determined using kallisto [Version 0.43.1]. We first created a transcriptome index in kallisto using Ensembl cDNA sequences for the reference genome. This index was then used to quantify transcript abundance in raw counts and counts per million (CPM). Differential expression (DE genes, FDR<0.05) was quantitated through DESeq2. PCA was conducted using ClustVis. Gene ontology pathway enrichment was conducted using the Gene Ontology analysis tool.

The conversion of RNA to cDNA was carried out with Superscript IV Vilo kit using 1µg of total RNA in a reaction volume of 20 µl as per manufacturer's instructions (Invitrogen #11766050). The reaction mixture in 4 µl consisting of Mgcl2, dNTP mix, Random primer and Reverse Transcriptase was set up with the remaining 16 µl with 1 ug of RNA with nuclease free water. The reverse transcription was carried out in the thermal cycler with the following steps, i.e., 25°C for 10 min, 55°C for 10 min, 85°C for 5 min and hold at 4°C. The 20 µl reaction mixture was

392 then reconstituted with Milli-Q water to 50 µl and used for further analysis. Quantitative RT-PCR reactions were
393 carried out in a volume of 20 µl of 1X SYBR Green fast qPCR Mix (#RK21200, ABclonal, Woburn, MA), and
394 100mM primers using CFX96 qPCR machine (Bio-Rad, Hercules, CA; thermal profile: 95C, 15sec; 60C, 30sec;
395 40X; melting curve). Comparative C(T) method which is also referred to as the 2-ΔΔCT method [63] was used
396 to determine the relative gene expression between the gene of interest relative to the internal housekeeping
397 control gene. The internal control gene used in the assays was GAPDH. Primers used for the analysis are listed
398 in Table1.

399 **Chromatin immunoprecipitation and sequencing**

400 Chromatin Immunoprecipitation (ChIP) was carried out using the skeletal muscle for the transcriptomic analysis.
401 The samples were chopped into small pieces and transferred to a tube containing 1ml of PBS with 27 µl of 37%
402 formaldehyde. The cross-linking process was carried out for 10 minutes on a rotator. After the incubation 50 µl
403 of 2.5 M glycine was added to each sample to a final concentration of 0.125 M and incubated for another 5
404 minutes to stop the cross-linking process. The samples were then centrifuged at 5000 rpm for 5 min to collect
405 and the supernatant was discarded without disturbing the pellet. The pellet was then washed by suspending in
406 ice-cold PBS and centrifuged at 5000 rpm for 5 minutes. This washing procedure was carried out three times.
407 The pellet was suspended in 1 ml of FA lysis buffer (50 mM HEPES, 140 mM NaCl, 1 mM ETDA, 1% Triton x-
408 100, 0.1% sodium deoxy cholate) containing protease inhibitor cocktail and 20% SDS and subjected to
409 sonication. Sonication of the chromatin fragmentation was performed using Bioruptor (Diagenode, Liège,
410 Belgium) with 45 on/off cycle for 10 minutes. After the sonication, the samples were centrifuged for 10 min at
411 14000 rpm to collect the supernatant/ lysate in a new tube. About 180 µl of the lysate was used for the
412 immunoprecipitation (IP) with the specific antibody listed in Table 2. Twenty percent of the IP was taken as input
413 and stored separately at -80°C for further use. The immunoprecipitation reaction of 500 µl consisting of the FA
414 lysis buffer with the protease inhibitor cocktail and the lysate was used for each sample. The respective
415 antibodies used are given in table 6 and an antibody concentration of 5 ug per sample was used. Pierce A/G
416 magnetic beads (Invitrogen # 80105G) of 30 µl were washed using FA lysis buffer 2 times and mixed with the IP
417 samples. The Immunoprecipitation reaction was carried out overnight on a rotator at 4 °C. After the incubation,
418 the beads were separated using the magnetic stand and the other lysate was discarded. The lysate was washed
419 with FA lysis buffer, high salt solution buffer, LiCl buffer and finally with TE buffer. The final elution was carried
420 out by suspending the beads in 100 µl of elution buffer and incubation on a shaking dry bath for 10 minutes at
421 70°C. The bead was separated on the magnetic stand and the renaming elution buffer containing the protein
422 DNA complex was collected in a separate tube. The input stored at -80 was used along with the IP samples. 4
423 µl of 5 M NaCl added to all samples and the reverse crosslinking were performed at 65°C overnight on shaking
424 dry bath. Following that, the DNA isolation was carried out as described in the DNA isolation protocol. Percentage
425 of Input, control and experimental samples were measured by qPCR analysis as described earlier. Primers were
426 selected among validated primer sets from the MGH Primer Bank; IDs: INS- 117606344c1; MYH7- 18859641a1;
427 MYH4- 9581821a1; MYH2-21489941a1; GR-6680103a1; Foxc1-410056a1; Arid5a-31542476a1; INSR-
428 67543660a1;IRS-29568118a1; GAPDH-6679937a1; PPARG-6755138a1; CEBPA-6680916a1; FATP1-

429 6755546a1; FABP4-14149635a1; CD36-31982474a1; ChIP-qPCR primers were manually designed using
430 primer 3 software: INSR F- ACCGCCACTACTTCTGCTAC; INSR R- CTTGGATCTAGGCCCGTGG; IRS F-
431 AAGGGGAGCAGGAGAAAAGG;IRS R- ACAAAAGGAGAACAGGGATCC;FABP4 F-
432 CTGTAGCCCGCATCCAGAG; FABP4 R- TTGGCTTTGTTTGGTTTGGG; CD36 F-
433 TAACCACCACAGCCATGAGT; CD36 R- CCACTTGGGGAAGCTGTTAG
434
435 For the ChIP sequence analysis, DNA purification with mini elute kit (Cat# 28004, QIAGEN, Hilden, Germany)
436 following quantification using Qubit ds DNA quantification assay kit (Invitrogen #Q32851) was done and DNA
437 concentration of 1ng was taken for analysis. Library preparation and sequencing were conducted at the CCHMC
438 Genomics Core, using TruSeq ChIP-seq library prep (with size exclusion) on ~10 ng of chromatin per ChIP
439 sample or pooled inputs and HiSeq 50-bp was conducted using HOMER software (v4.10) after aligning fastq
440 files to the mm10 mouse genome using bowtie2. PCA was conducted using ClustVis. Heatmaps of peak density
441 were imaged with TreeView3. Peak tracks were imaged through WashU epigenome browser. Gene ontology
442 pathway enrichment was conducted using the gene ontology analysis tool.

443 **Total protein isolation, Western blotting and Co-immunoprecipitation**

444 Total protein isolation was carried out from skeletal muscle (soleus and gastrocnemius) tissues. About 100 mg
445 of tissues were weighed and chopped into small pieces using a sterile blade and transferred to a 2 ml sterile
446 Eppendorf tube. To each sample, 1 ml of RIPA lysis buffer was added. The RIPA buffer preparation includes 1
447 X PBS, 50 mM NaF, 0.5% Na deoxycholate (w/v), 0.1% SDS, 1% IGEPAL, 1.5 mM Na3VO4, 1 mM PMSF and
448 complete protease inhibitor (Roche Molecular Biochemicals, IN, USA). The samples were kept on ice and
449 homogenized using a homogenizer. After the homogenization, the sample mixtures were incubated on ice for
450 10min followed by centrifugation at 10,000 rpm for 10 min at 4°C. The supernatant was collected in a sterile
451 Eppendorf tube and was quantitated with Bio-Rad protein micro assay using BSA as standard (Cat no. 500-
452 0001). The protein sample of 1ul and the corresponding amount of BSA standard were added to Tris-Hcl solution
453 and then to Bio-Rad dye on a micro titer plate. The plate was then incubated in the spectrophotometer for 30min
454 and the absorbance at 595 nm was recorded. The OD value of the sample and BSA standard were plotted, and
455 the concentration of samples was determined. Based on the concentration, each sample was prepared (5 ug/1
456 ul) for western blot by adding the sample to 4 X loading dye and heated the mixture at 100°C for 10 min.

457 Western blotting was done using 10% SDS-PAGE gels. The protein amount of 20 to 80 ug was loaded per lane
458 depending on the target protein and experiments. The SDS PAGE gels were subjected to electrophoresis at 90
459 V for 90 min with 1 X MOPS running buffer. 10 µl of prestained protein ladder was loaded along with the sample
460 to identify the molecular weight of proteins of interest. The bromophenol blue in the loading buffer was used as
461 the tracking dye. Once the run was complete, the gel was transferred to a PVDF membrane (0.4 um) by wet
462 transfer. The gel, PVDF membrane along with the filter papers and sponges were arranged as a sandwich and
463 placed in the transfer tank with 1 X transfer buffer. The wet transfer was carried out at 100 V for 1 hr or at 30 V
464 for overnight for high molecular weight proteins. On completion of the transfer, the membrane was stained with
465 ponceau stain to check for proper transfer of bands on the membrane. The membrane was blocked with 5%

466 nonfat dry milk in TBST. The primary antibody was added to the 5% nonfat dry milk on the membrane at
467 respective concentration and incubated overnight at 4°C with shaking. The membrane was washed with 5%milk
468 three times for 10 min each and incubated with secondary antibody for 1 hr at room temperature on a shaker.
469 After the incubation, the membranes were washed three times with 5% milk for 10 min each. In the last step, the
470 detection of chemiluminescence was achieved by incubation of the membrane with a substrate such as
471 SuperSignal™ West Femto Maximum Sensitivity Substrate (34094, Thermo Scientific) or SuperSignal™ West
472 Pico PLUS Chemiluminescent Substrate (34577, Thermo Scientific). The substrate was removed, and the
473 membrane was visualized using the Bio-Rad chemiDoc system (Biorad #12003153**)**. Information of the specific
474 antibodies used at 1:1000 dilution:): rabbit anti-GAPDH (ABClonal #A19056), rabbit anti-GR (ABClonal #A2164),
475 rabbit anti-HISTONE H3 (ABClonal #A20822), rabbit anti-FOXC1 (ABClonal #A2924), rabbit anti-ARID5a
476 (Invitrogen MA518292), rabbit anti-Phospho IRS (S307) (ABClonal #AP0371), rabbit anti-IRS (ABClonal
477 #A19245), rabbit anti-AKT (ABClonal #A22533), rabbit anti-Phospho AKT (s473) (ABClonal #AP0098), rabbit
478 anti-GLUT4 (ABClonal #A7637), rabbit anti-INSR (ABClonal #A16900), rabbit anti-FABP4 (ABClonal #A11481),
479 rabbit anti-CD36 (ABClonal #A5792), rabbit anti-HDAC1 (ABClonal #A0238), rabbit anti-SIN3A (ABClonal
480 #A1577), rabbit anti-MYH4 (ABClonal #A15293), rabbit anti-MYH2 (ABClonal #A15292), rabbit anti-MYH7
481 (ABClonal #A7564), mouse anti-OXOPHOS (Abcam #ab110413). rabbit anti-PPARG (Invitrogen PA3-821A),
482 rabbit anti-SAP30 (Invitrogen PA5-103284. Secondary antibody (diluted 1:3000 dilution): HRP-conjugated
483 donkey anti-rabbit or anti-mouse (#sc-2313 and #sc-2314, Santa Cruz Biotech, Dallas, TX).

484 Co-immunoprecipitation analysis from the total protein isolated from muscle was assessed for protein complex
485 interaction and difference in interaction among each group of GR $^{wt/wt}$ and GR $^{R24K/R24K}$ mice at adult. The Co-
486 immunoprecipitation (Co-IP) protocol includes pulling down the protein complex with an antibody against one
487 member of the complex and coupling the antibody to a magnetic bead, followed by the isolation and elution of
488 the complex and then verification by western blot analysis of each protein complex moieties. The universal
489 magnetic Co-IP kit (Active motif, 54002, Carlsbad, CA, USA) was used and the appropriate antibodies (specified
490 in table 2) and the control IgG of 2 µg were used to pull down the complex. The total protein extract of 800 µg
491 was prepared in a final volume of 500 ul, with the complete Co-IP/Wash buffer and incubated with the specific
492 antibodies and IgG control overnight at 4°C on a rotator. After the incubation, the protein G magnetic beads
493 (Invitrogen # 80105G) were added to the mixture and incubated at room temperature for 1 hr. The magnetic
494 beads were then separated using a magnetic separator and the mixture was discarded. The magnetic beads
495 which hold the corresponding complex were then washed with IP wash buffer three times and the final elution
496 was done by suspending the beads in 50 µl of 2 X loading dye. The beads were headed at 100°C for 5 min. The
497 protein complexes and the beads were then separated using the magnetic stand and loading dye with the
498 proteins were separated into a new tube and the samples were loaded onto a 10% SDS- PAGE gel with 20 µl
499 loaded each lane.

500 **Nuclear, cytoplasmic and membrane fraction analysis**

501 The separation of nuclear and cytoplasmic protein analysis was performed using NE-PER nuclear and
502 cytoplasmic extraction kit (Invitrogen #78835). Briefly, 100mg of the skeletal muscle was homogenized and 1ml

503 of CERI solution was added and vortexed vigorously on high setting for 15sec. Following incubation on ice for
504 10 min 55ul of ice cold CERII solution was added, vortexed, incubated for a minute and centrifuged for 5 min at
505 16,000g. The supernatant containing the cytoplasmic fraction was separated into a new 1.5 Eppendorf tube and
506 then suspended the insoluble pellet with 500ul of ice-cold NER solution. The sample was placed on ice for 40
507 minutes and vortexed every 10 for 1 sec. Finally, the samples were centrifuged for 10 min at 16,000g and the
508 supernatant containing the nuclear fraction was separated and in a new 1.5 Eppendorf tube and stored at -80C
509 until use.

510 The isolation of membrane proteins was achieved by a modified protocol [64]. Muscle tissue (50 mg) from day 1
511 ABW and LBW pups were taken and cut into pieces using a sterile blade and transferred to 2 ml Eppendorf tube
512 containing the homogenizing buffer [39 ml Buffer A (121.10 mg Tris- base, 37.22 mg EDTA per 100 ml of dd
513 H2o, at pH 7.4), 13 ml of 20 µm EDTA in buffer A and 312 µl of PMSF], 3 ml of buffer 1 (43.5 g KCl, 13.0 g tetra-
514 sodium pyrophosphate in 500 ml of dd H20). The tissue was homogenized using a homogenizer and the mixture
515 was incubated on ice for 15 min. After the incubation, the samples were centrifuged in an ultracentrifuge at
516 50,000 rpm for 45 min at 4oC. The pellet was washed in 1 ml of buffer 2 (121.10 mg Tris- base, 37.22 mg EDTA
517 in 100 ml of dd H2O at pH 7.4) and the solution was discarded without disturbing the pellet and the tube was
518 dried with a cotton bud. The pellet was homogenized in 600 µl buffer 2, 200 µl 16% SDS was added and
519 centrifuged at 3000 rpm for 20 min at 20º C. The supernatant was collected, and the protein concentration was
520 determined by Bio-Rad protein assay as described previously. Once the protein concentration was determined,
521 western blotting analysis was carried out as previously described.

522 **Protein Immunoprecipitation following LC-MS/ MS analyses.**

523 Immunoprecipitation of proteins without the contaminant of antibody heavy and light chain through bead antibody
524 conjugation was carried out using the Pierce Co-IP kit (Invitrogen #26149). Briefly, the antibody of 10-75ug was
525 conjugated with the amino link plus coupling resin using the coupling buffer containing the sodium
526 cyanoborohydride as conjugation reagent was performed in 1.5ml Eppendorf tube in a thermomixer incubated
527 at room temperature for 2 hours. Simultaneously, the protein extracts were pre-cleared with control agarose
528 resins for 1 hour. Then resin was washed with serial solutions of quenching and wash buffers. The eluted pre -
529 cleared protein extracts were added onto the antibody conjugated amino link resin at 4C overnight following
530 which the interaction was washed with was buffer the following day and eluted using 50ul of elution buffer. The
531 eluted protein was run on SDS-PAGE silver stained and western analysis were carried out to confirm the
532 existence of antibody elution following which the samples were submitted to the LC-MS/ MS protein core at UC.

533 The protein samples were dried by speed vac and resuspended in 35 µl of 1X LB. The samples were then run
534 1.5cm into an Invitrogen 4-12% B-T gel using MOPS buffer with molecular weight marker lanes in between.
535 The sections were excised, reduced with DTT, alkylated with IAA and digested with trypsin overnight. The
536 resulting peptides were extracted and dried by speed vac. They were then resuspended in 0.1% Formic acid
537 (FA). 500ng- 2 ug of each sample was analyzed by nano LC-MS/MS (Orbitrap Eclipse) and was searched against

538 a combined database of a combined contaminants database and the Swissport Mus musculus database using
539 Proteome discoverer version 3.0 with the Sequest HT search algorithm (Thermoscientific).

540 **Immunostaining**

541 Excised muscle tissues were fixed in 10% formaldehyde (Cat #245-684; Fisher Scientific, Waltham, MA) at room
542 temperature for ~24 hours, then stored at +4C before processing. Tissue sections of 5–7 μm thickness of was
543 stained with hematoxylin and eosin (H&E; cat #12013B, 1070C; Newcomer Supply, Middleton, WI). CSA
544 quantitation was conducted on >400 myofibers per tissue per mouse. Imaging was performed using an Axio
545 Observer A1 microscope (Zeiss, Oberkochen, Germany), using 10X and 20X (short-range) objectives. Images
546 were acquired through Gryphax software (version 1.0.6.598; Jenoptik, Jena, Germany) and quantitated through
547 ImageJ [65]. In case of myofiber typing, sections were incubated with primary antibodies BA-F8 (1:10), SC-71
548 (1:30) and BF-F3 (1:10; all by Developmental Studies Hybridoma Bank, Iowa City, IA) overnight at 4°C. Then,
549 sections were incubated with secondary antibodies AlexaFluor350 anti-IgG2b, AlexaFluor488 anti-IgG1 and
550 AlexaFluor594 anti-IgM (Cat #A21140, A21121, 1010111; Life Technologies, Grand Island, NY). Type 1 fibers
551 stained blue, type 2A stained green, type 2X showed no staining, type 2B stained red. Myofiber types were then
552 quantitated over at least five serial sections and quantitated as % of total counted myofibers.

553 **Cell culture and gene overexpression analyses**

554 The C2C12 skeletal muscle cell lines, both the wild type and transfected were maintained on DMEM
555 supplemented with 10% fetal bovine serum and 1% Pen strep in 5%CO2 at 37C incubator. When the cells
556 reached 80% confluency, they were transfected using the Lipofectamine 3000 transfection reagent (Invitrogen
557 #L3000015) with plasmid carrying the gene of interest (Foxc1 and Arid5a). After 48 hours of transfection the
558 cells were washed with PBS and RNA and Proteins were extracted as described and assessed for gene of
559 interest overexpression and its associated targets.

560 **Analyses of body composition and muscle function**

561 Our routine procedures concerning body composition, muscle function, mass and myofiber typing can be found
562 as point-by-point protocols here [66].

563 Forelimb grip strength was monitored using a meter (#1027SM; Columbus Instruments, Columbus, OH) blinded
564 to treatment groups. Animals performed ten pulls with 5 seconds rest on a flat surface between pulls. Grip
565 strength was expressed as force normalized to body weight. Running endurance was tested on a motorized
566 treadmill with electrified resting posts (#1050RM, Columbus Instruments, Columbus, OH) and 10° inclination.
567 Speed was accelerated at 1m/min2 starting at 1m/min and individual test was interrupted when the subject spent
568 >30sec on resting post. Running endurance was analyzed as weight-normalized cumulative work (mW)[67].

569 Immediately prior to sacrifice, in situ tetanic force from tibialis anterior muscle was measured using a Whole
570 Mouse Test System (Cat #1300A; Aurora Scientific, Aurora, ON, Canada) with a 1N dual-action lever arm force
571 transducer (300C-LR, Aurora Scientific, Aurora, ON, Canada) in anesthetized animals (0.8 l/min of 1.5%

572 isoflurane in 100% O2). Specifications of tetanic isometric contraction: initial delay, 0.1 sec; frequency, 200Hz;
573 pulse width, 0.5 msec; duration, 0.5 sec; stimulation, 100mA [68]. Muscle length was adjusted to a fixed baseline
574 of ~50mN resting tension for all muscles/conditions. Force-frequency curve was measured from 25 Hz to 200
575 Hz with intervals of 25 Hz, pause 1 minute between tetani. Fatigue analysis was conducted by repeating tetanic
576 contractions every 10 seconds until complete exhaustion of the muscle (50 cycles). Specific force was calculated
577 (N/mm2) for each tetanus frequency as (P0 N)/[(muscle mass mg/1.06 mg/mm3)/Lf mm]. 1.06 mg/mm3 is the
578 mammalian muscle density. Lf=L0*0.6, where 0.6 is the muscle to fiber length ratio in tibialis anterior muscle
579 [69]. We reported here specific force values in N/cm2 units.

580 Magnetic resonance imaging (MRI) scans to determine lean mass ratios (% of total body mass) were conducted
581 in non-anesthetized, non-fasted mice at ZT8 using the EchoMRI-100H Whole Body Composition analyzer
582 (EchoMRI, Houston, TX). Mice were weighed immediately prior to MRI scan. Before each measurement
583 session, the system was calibrated using the standard internal calibrator tube (canola oil). Mice were scanned
584 in sample tubes dedicated to mice comprised between 20 g and 40 g body mass. Data were collected through
585 built-in software EchoMRI version 140320. Data were analyzed when hydration ratio > 85 %.

586 Muscle mass was calculated as muscle weight immediately after sacrifice and explant, normalized to whole body
587 weight.

588 **Respirometry with isolated mitochondria and muscle tissue**

589 Basal tissue OCR values were obtained from basal rates of oxygen consumption of muscle biopsies at the
590 Seahorse XF HS Mini Extracellular Flux Analyzer platform (Agilent, Santa Clara, CA) using previously detailed
591 conditions [68]. Basal OCR was calculated as baseline value (average of 3 consecutive reads) minus value after
592 rotenone/antimycin addition (average of 3 consecutive reads). Basal OCR values were normalized to total protein
593 content, assayed in each well after the Seahorse through homogenization and Bradford assay. Nutrients: 5mM
594 glucose, 1mM palmitate-BSA (#G7021, #P0500; Millipore-Sigma, St Louis, MO); inhibitors: 0.5mM rotenone +
595 0.5mM antimycin A (Agilent).

596 Respiratory control ratio (RCR) values were obtained from isolated mitochondria from muscle tissue. Quadriceps
597 are harvested from the mouse and cut into very fine pieces. The minced tissue is placed in a 15mL conical tube
598 (USA Scientific #188261) and 5mL of MS-EGTA buffer with 1mg Trypsin (Sigma #T1426-50MG) is added to the
599 tube. The tube is quickly vortexed, and the tissue is left submerged in the solution. After 2 minutes, 5mL of MS-
600 EGTA buffer with 0.2% BSA (Goldbio #A-421-250) is added to the tube to stop the trypsin reaction. MS-EGTA
601 buffer: Mannitol- ChemProducts #M0214-45, Sucrose- Millipore #100892, HEPES- Gibco #15630-080, EGTA-
602 RPI #E14100-50.0. The tube is inverted several times to mix then set to rest. Once the tissue has mostly settled
603 to the bottom of the tube, 3mL of buffer is aspirated and the remaining solution and tissue is transferred to a
604 10mL glass tissue homogenizer (Avantor # 89026-382). Once sufficiently homogenized the solution is
605 transferred back into the 15mL conical tube and spun in the centrifuge at 1,000g for 5 minutes at 4 degrees
606 Celsius. After spinning, the supernatant is transferred to a new 15mL conical tube. The supernatant in the new
607 tube is then centrifuged at 12,000g for 10 minutes at 4 degrees Celsius to pellet the mitochondria. The

608 supernatant is discarded from the pellet and the pellet is then resuspended in 7mL of MS-EGTA buffer and
609 centrifuged again at 12,000g for 10 minutes at 4 degrees Celsius. After spinning, the supernatant is discarded,
610 and the mitochondria are resuspended in 1mL of Seahorse medium (Agilent #103335-100) with supplemented
611 10µL of 5mM pyruvate (Sigma #P2256-100G) and 10µL of 5mM malate (Cayman Chemical #20765). After
612 protein quantitation using a Bradford assay (Bio-Rad #5000001), 2.5µg mitochondria are dispensed per well in
613 180µl total volumes and let to equilibrate for 1 hour at 37°C. 20µL of 5mM ADP (Sigma #01905), 50µM
614 Oligomycin (Millipore #495455-10MG), 100µM Carbonyl cyanide-p-trifluoromethoxy phenylhydrazone (TCI
615 #C3463), and 5µM Rotenone (Millipore #557368-1GM)/Antimycin A (Sigma #A674-50MG) are added to drug
616 ports A, B, C, and D respectively to yield final concentrations of 0.5mM, 50µM, 10µM, and 0.5µM. Nutrients:
617 0.5mM pyruvate, 0.1mM palmitoyl carnitine (#P2256, #61251; Millipore-Sigma, St Louis, MO). At baseline and
618 after each drug injection, samples are read three consecutive times. RCR was calculated as the ratio between
619 state III (OCR after ADP addition) and uncoupled state IV (OCR after oligomycin addition). Seahorse
620 measurements were conducted blinded to treatment groups.

621 **Metabolic cages and metabolic treadmill**

622 VO2 in baseline conditions (ml/h; expressed as aggregate values of l/day) was assessed via indirect calorimetry
623 using the Promethean Automated Phenotyping System (Sable Systems International, Las Vegas, NV) at the
624 shared Metabolic Cage facility in the CCHMC Vet Services. Data collection lasted for 5 days. Results are
625 expressed as average values (all mice per group, all values per mouse, average of 5 days) over a circadian
626 period, as well as in an ANCOVA analysis (test for difference in regression lines; performed through CalR[70])
627 with average values of active phase plotted against body mass values per mouse, as recommended by [71].

628 For VO2 analysis during aerobic exercise, we used an Oxymax Metabolic Treadmill (Columbus Instruments,
629 Columbus, OH), using the stepwise speed increase protocol described previously to separate young vs aged
630 mice based on the slope of the VO2/workload curve and VO2 rates at baseline, submaximal and maximal (75%)
631 workloads [72]. The treadmill belt was angled 10° uphill to match our regular treadmill conditions and calculate
632 work. Mice were assessed at the metabolic treadmill at 24hours after the last vehicle or prednisone injection.
633 Metabolic cage and metabolic treadmill assessments were performed blinded to regimens or genotype.

634 **AAV preparation**

635 Approximately 70-80% confluent HEK293T cells (AAVpro® 293T Cell Line; Takara # 632273 AAVpro® 293T
636 Cell Line; Takara # 632273) in DMEM (SH30022.01, Cytiva Life Sciences) supplemented with 2% Bovine Growth
637 Serum (BGS; Cytiva Life Sciences), and 1.0 mM Sodium Pyruvate were triple transfected with pHelper (Cell
638 Biolabs;340202), pAAV-GOI (Vector Builder; (VB230825-1437xmg; pAAV[Exp]-CMV>{mFoxc1[NM_008592.2]*-
639 3xFLAG:WPRE), VB230825-1437xmg; pAAV[Exp]-CMV>{mArid5a[NM_001290726.1]*-3xFLAG:WPRE)) and
640 pAAV Rep-Cap (1A-Myo; Gift of Molkentin Lab) plasmids using PEI, Linear, MW250,000 (PolySciences, Inc) in
641 40-T150mm cell culture plates. Eighteen hours after transfection, medium is changed to DMEM supplemented
642 with 1% BGS, 1.0 mM Sodium Pyruvate, and 1X MEM Non-essential Amino Acid Solution (Sigma; M7148).
643 Approximately 96 hours post-transfection, the media and cells were collected and processed separately. Cells

644 were lysed using repeated freeze/thaw cycles at a minimum of five times in 1X Gradient Buffer (0.1 M Tris, 0.5
645 M NaCl, 0.1 M MgCl2). The cell debris were then treated with Benzonase Endonuclease at 0.65 µl per 5 mL
646 (Sigma-Aldrich #1037731010 (100000 Units)) for at least one hour. The homogenates were cleared from debris
647 by centrifugation. AAVs were precipitated from the cell medium with polyethylene glycol (PEG) 8000 The PEG-
648 precipitated AAV was collected by centrifugation, and the AAV pellet was resuspended in 1X GB. Media and cell
649 AAV's were combined and AAV's were purified using an Iodixanol (Opti Prep Density Gradient Medium; Sigma-
650 Aldrich #D1556250) gradient at 15%, 25%, 40% and 60% in 1XGB. The AAV band was removed and purified
651 using Centrifugal Filters (30000 NMWL (30K), 4.0 mL Sample Volume; Millipore-Sigma #UFC803024, and
652 100000 NMWL (100K), 15.0 mL Sample Volume; Millipore-Sigma # UFC910024) in a2X PBS, 10mM MgCl2
653 solution.

654 **Viral titration**

655 Primer's binding within the AAV-GOI ITR's CMV region (Forward: GTTCCGCGTTACATAACTTACGG; Reverse:
656 CTGCCAAGTGGGCAGTTTACC) were used to measure the virus titer with quantitative polymerase chain
657 reaction (qPCR). Before releasing the viral DNA from the particles, all extra-viral DNA was removed by digestion
658 with DNase I. Then, the viral DNA was released by Proteinase K digestion.

659 **In vivo viral injection**

660 The viral load of MyoAAV's corresponding to 10^12 per construct per mouse were administered retro-orbitally in
661 anesthetized mice. Muscles were then excised after 2 weeks for immediate sufficiency proofs, or after 12 weeks
662 in combination with high-fat diet for sufficiency proofs in the presence of metabolic stress.

663 **Statistics and UK Biobank analyses**

664 Statistical analyses were performed using Prism software v9.2.0 (GraphPad, La Jolla, CA). The Pearson-
665 D'Agostino normality test was used to assess data distribution normality. When comparing data groups for more
666 than one related variable, two-way ANOVA was used with Sidak multi-comparison (treatment vs age effect;
667 treatment vs KO effect). Significance scores reported on charts: *, P<0.05; **, P<0.01; ***, P<0.001; ****,
668 P<0.0001. When the number of data points was less than 10, data were presented as single values (dot plots,
669 histograms). Tukey distribution bars or violin plots were used to emphasize data range distribution in analyses
670 pooling larger data point sets per group (typically > 10 data points). For curves, the s.e.m. values for each plotted
671 point were reported as upper and lower lines.

672 Our UK Biobank study was conducted under the UKB application number 65846. We constructed a rs6190
673 genotype-stratified cohort, excluding participants if they withdrew consent. All available values for the tested
674 parameters were collected per genotype group. Hand grip strength values were analyzed as max hand grip
675 strength (right or left) normalized to ipsilateral arm lean mass. UDI and related parameters: Age: 21001-0.0; BMI:
676 21001-0.0; Glycemia (mM): 30740-0.0; whole body lean mass (kg): 23101-0.0; hand grip strength right (kg): 47-
677 0.0; arm lean mass kg (right): 23121-0.0; Hand grip strength left (kg): 46-0.0; arm lean mass kg (left): 23125-0.0.
678 For independent association studies, multiple linear regression analysis was carried out using R 4.3.2 (R Core

679 Team, 2023) to explore the association of rs6190 genotype with sex-disaggregated male data of BMI, glycemia
680 and hand grip strength. For the cross-sectional comparisons of homozygous SNP carriers vs non-carriers, single-
681 pass ROUT was used to remove outliers and normality was tested with Pearson-D'Agostino. Because the data
682 distribution was not normal, Mann-Whitney U test was used for two-group comparisons, whereas Kruskal-Wallis
683 + Dunn's multi-comparison was used for three-group comparisons. In both cases, a $P<0.05$ was considered
684 significant.

685

young adult male mice (4mo ♂) GR$^{wt/wt}$ GR$^{R24K/R24K}$

**A**

rs6190 -> p.R23K

human GR

aa1-24 MDSKESLTP-GREENPSSVLAQERG

aa1-25 MDSKESLAPPGRDEVPSSLLGRGRG

murine GR

rs6190 ortholog -> p.R24K

SNP in target codon

AGG -> AAG

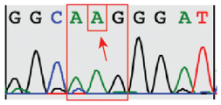


murine *Nr3c1* locus (exon 2)

G/G genotype = GR$^{wt/wt}$

A/A genotype = GR$^{R24K/R24K}$

CRISPR-Knock-in in mice

GR$^{wt/wt}$ GR$^{R24K/R24K}$

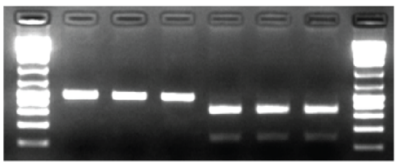

GR$^{wt}$ amplicon + BamHI = 474bp

GR$^{R24K}$ amplicon + BamHI = 334 + 140 bp

**B** body composition

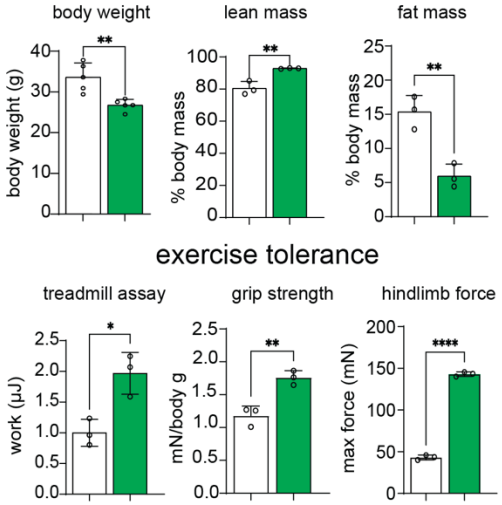


**C** glucose homeostasis

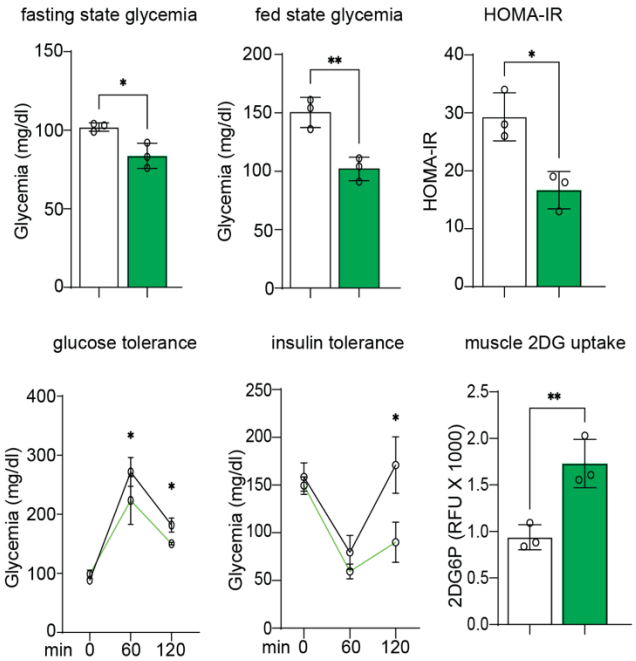


**D** myofiber typing (gastrocnemius)

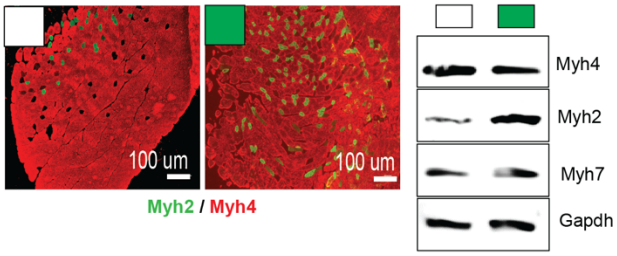


qPCR analysis

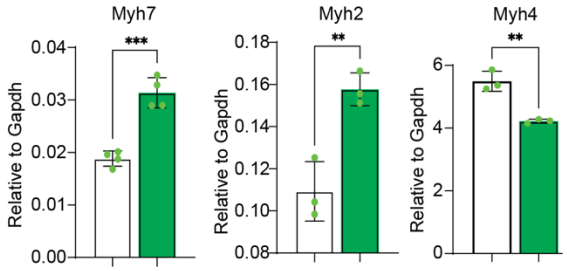


**E** myofiber CSA (gastrocnemius)

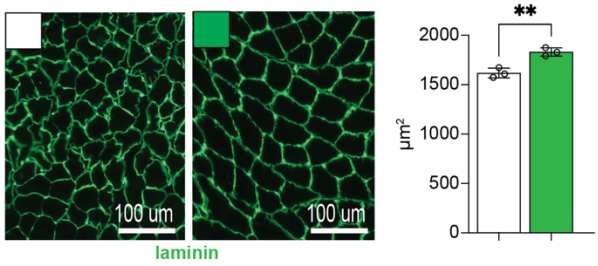


**F** mitochondrial respiration and mitochondrial complex protein levels

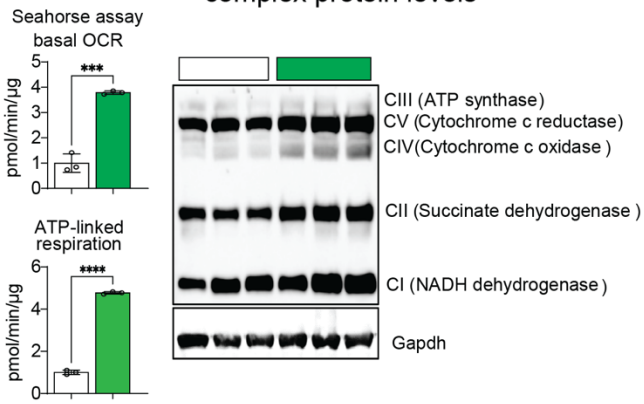

687 **Figure1. $GR^{R24k/R24k}$ mice exhibit leaner body composition and increased exercise tolerance. (A)**. The
688 CRISPR-mediated transgenic knock-in mutant GR mice validation through PCR-RFLP. **(B).** Mutant GR mice
689 exhibited leaner body composition and increased performance at treadmill, grip strength and force tests. **(C).**
690 Glucose homeostasis and muscle 2DG uptake (surrogate measure of glucose uptake) were improved in mutant
691 mice**. (D).** Immunostaining, WB and qPCR analysis showed gain of oxidative myofiber switch in mutant muscle**.**
692 **(E).** Mutant muscle showed increased average cross-sectional area (CSA). **(F).** Seahorse analysis revealed
693 increased levels of basal OCR and ATP-linked respiration in muscle biopsies, while WB showed gain of
694 mitochondrial complex signal in muscle tissue of mutant mice compared to WT littermates. N=3-5/group; Welch's
695 t-test (histograms), 2w ANOVA + Sidak (curves); *, P<0.05; **, P<0.01; ***, P<0.001; ****, P<0.0001.

young adult male mice (4mo ♂) GR$^{wt/wt}$ GR$^{R24K/R24K}$

**A** GR protein interactors through IP-MS analysis

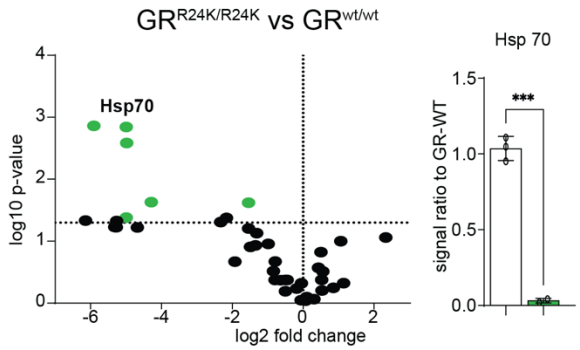


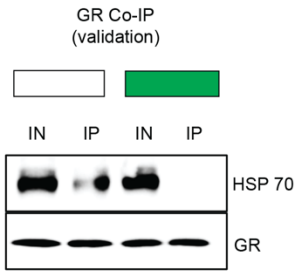


**B** GR translocation (+ dexamethasone)

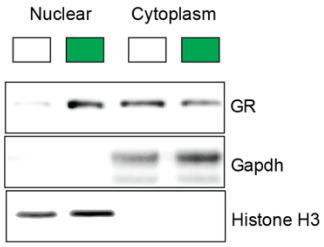


**C**

canonical reporter of GR epigenomic activity

top enriched motif

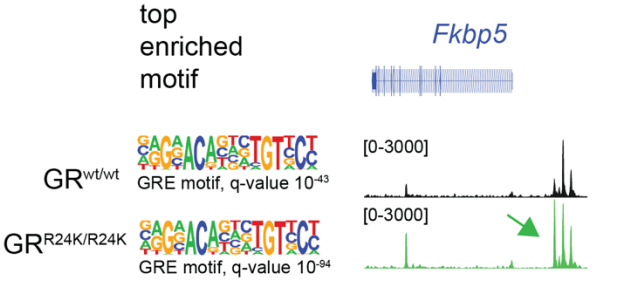


GR signal on GRE motifs (genome-wide)

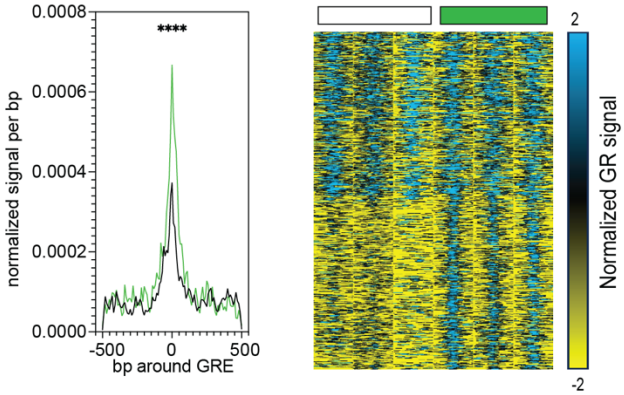


genomic location of GR peaks

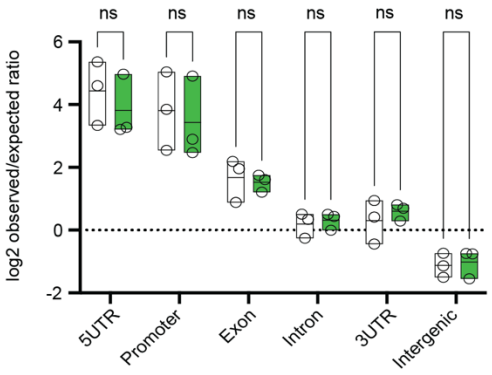


**D** ChIP-seq overlay with RNA-seq (quadriceps muscle)

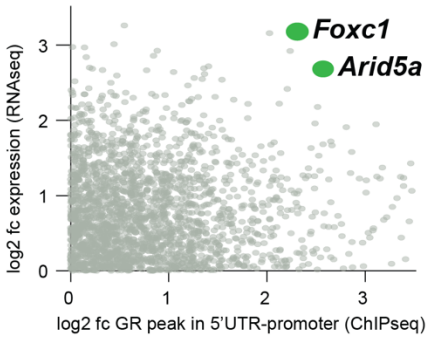


**E** GR peak profiles for *Foxc1* and *Arid5a*

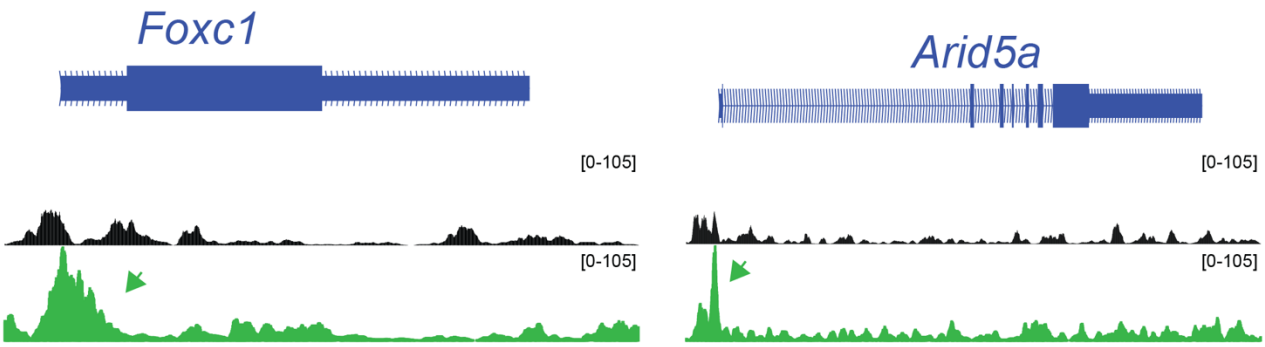


696

697 **Figure2. The mutant GR shows increased transactivation activity in muscle. (A).** IP-MS analysis of wild
698 type and mutant muscles revealed decreased binding of the mutant GR for Hsp70, confirmed through CoIP. **(B).**
699 Upon glucocorticoid stimulation in vivo, the muscle mutant GR showed increased nuclear translocation
700 compared to WT GR. (C). Muscle ChIP-seq revealed increased epigenomic GR activity with maintained peak
701 enrichment in 5'UTR-promoter regions for the mutant GR. **(D).** ChIP-seq overlay with RNA-seq revealed *Foxc1*
702 and *Arid5a* as top transactivation targets of the mutant GR**. (E)** GR peak profiles showed gain of mutant GR
703 signal on proximal promoter regions for both genes. N=3-5/group; Welch's t-test (A, histogram); 2w ANOVA +
704 Sidak (C); *, P<0.05; **, P<0.01; ***, P<0.001; ****, P<0.0001.

705

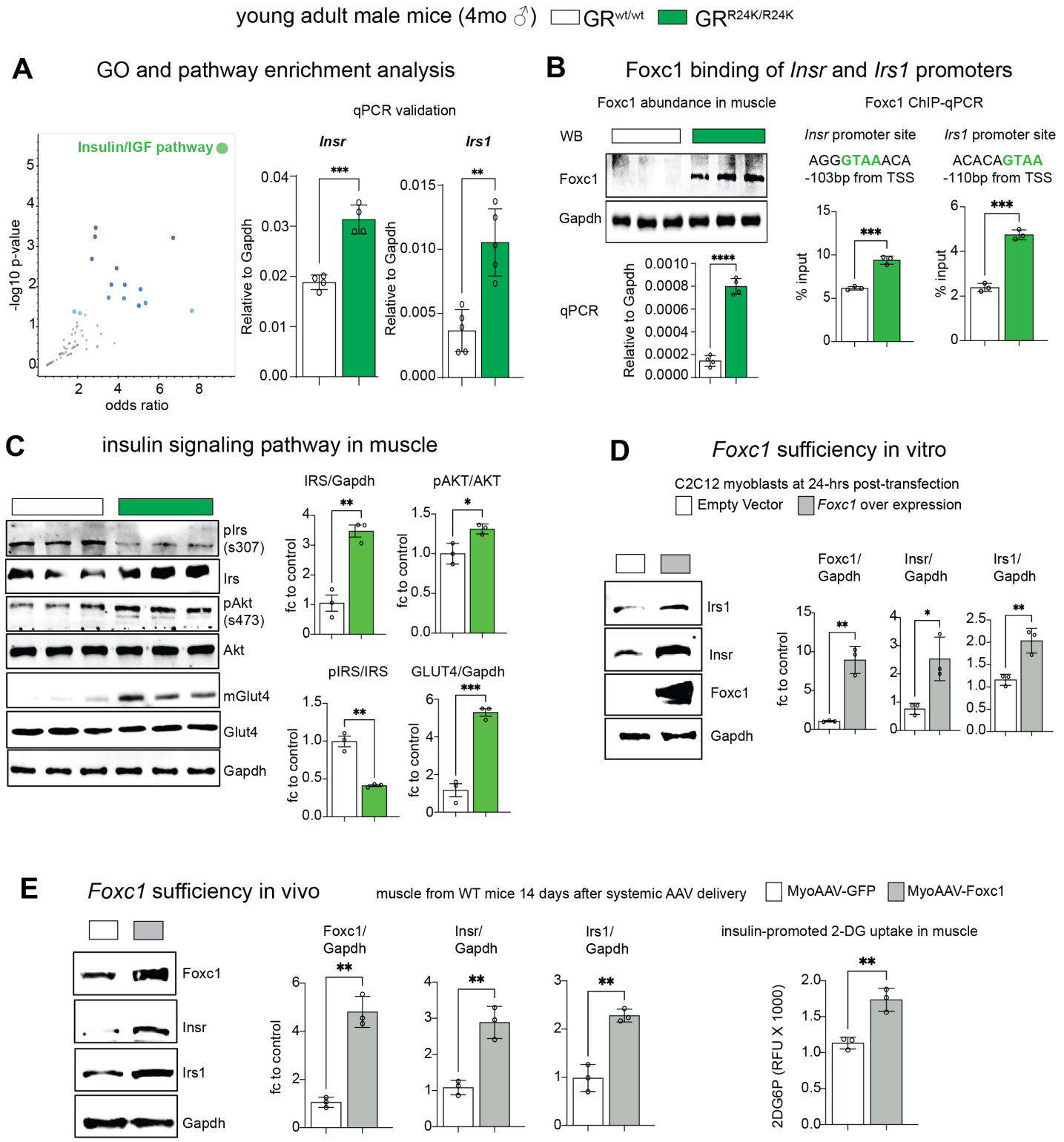


**Figure 3. Foxc1 is sufficient to promote *Insr/Irs1* expression and muscle insulin sensitivity. (A).** GO analysis of RNA-seq and qPCR validation revealed *Insr* and *Irs1* gene upregulation in muscle by the mutant GR. **(B).** Mutant muscle upregulated Foxc1 levels and its binding of canonical sites on the proximal promoter regions of *Insr* and *Irs1*. **(C).** WB analysis of whole and phosphorylated proteins showed increased activation of the insulin response pathway in the mutant muscle compared to control. **(D)** Validation of Foxc1-driven transactivation of Insr and Irs1 in C2C12 myoblasts in vitro. **(E).** In vivo AAV-based transduction showed that Foxc1 overexpression in muscle was sufficient to increase overall abundance of Insr and Irs1, increasing insulin-promoted 2DG uptake in vivo. N=3-5/group; Welch's t-test; *, P<0.05; **, P<0.01; ***, P<0.001; ****, P<0.0001.

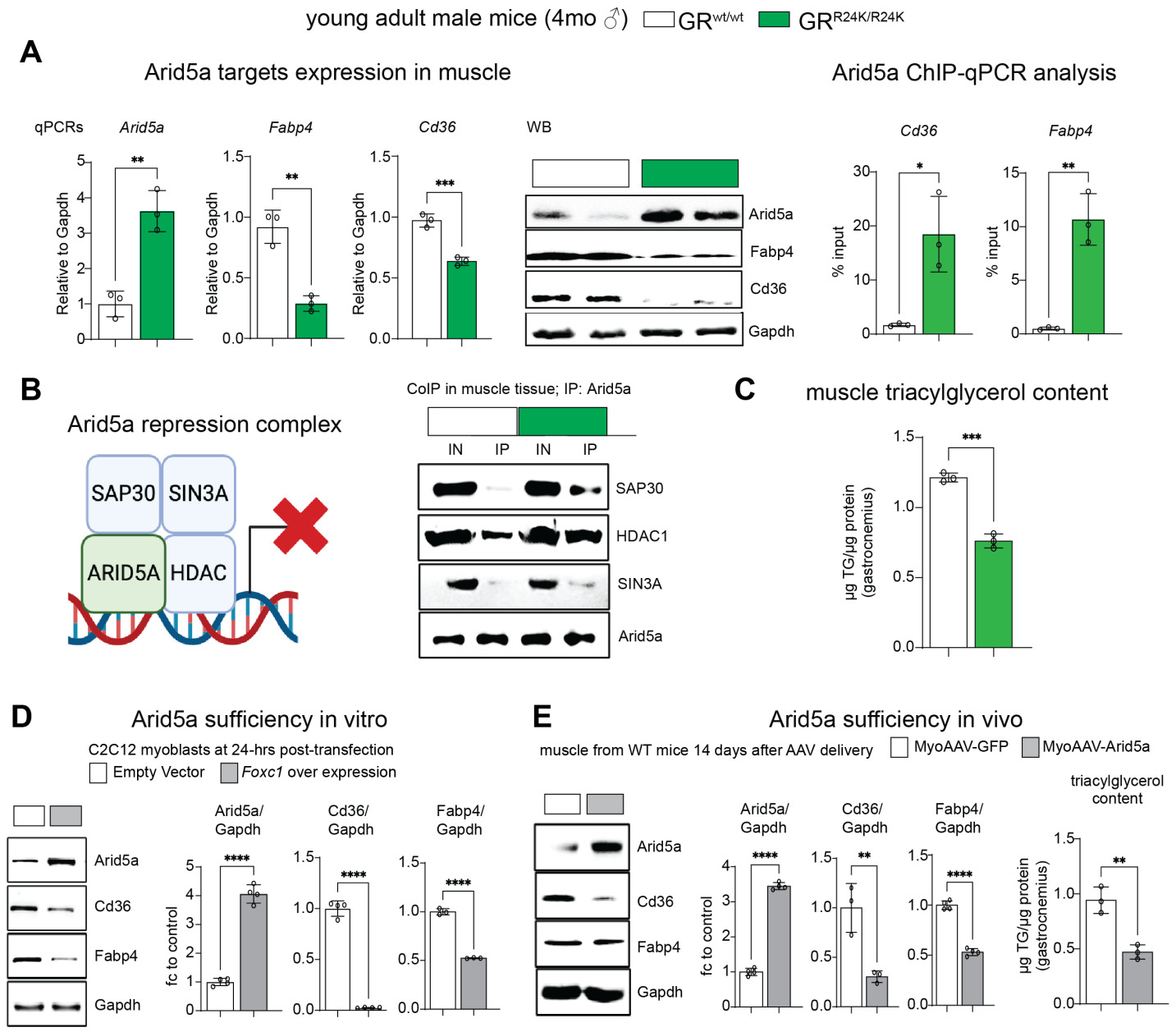


**Figure 4: Arid5a is sufficient to repress *Cd36/Fabp4* expression and muscle triacylglycerol content. (A).** Arid5a upregulation in mutant muscle correlated with downregulation of lipid transporter genes Cd36 and Fabp4, which showed increased Arid5a occupancy on their proximal promoters. **(B).** CoIP assays in muscle tissue showed increased interaction of Arid5a with its repression complex co-factors in the mutant muscle compared to control. **(C).** Triacylglycerol content in mutant muscle was lower than control. **(D)** Validation of Arid5a-driven transrepression of Cd36 and Fabp4 in C2C12 myoblasts in vitro. **(E).** In vivo AAV-based transduction showed that Arid5a overexpression in muscle was sufficient to decrease Cd36, Fabp4 and triacylglyerol content in muscle. N=3-4/group; Welch's t-test; *, P<0.05; **, P<0.01; ***, P<0.001; ****, P<0.0001.

young adult male mice (4mo ♂) with high-fat diet (60% kcal from fat) GR$^{wt/wt}$ GR$^{R24K/R24K}$

**A** Growth trajectories and body composition

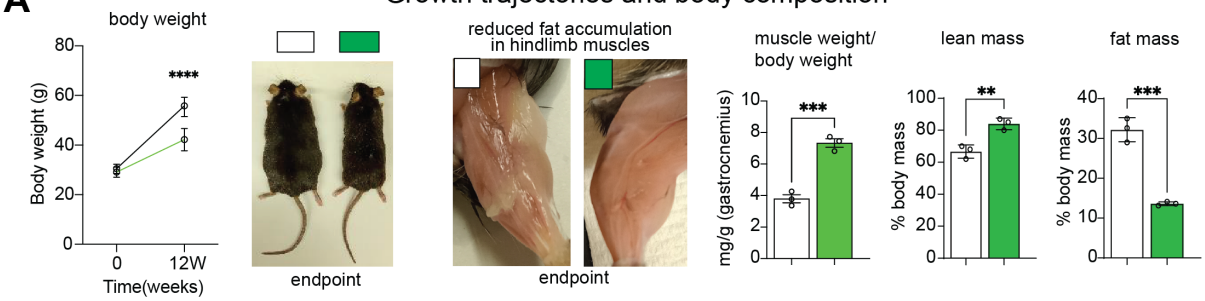


**B** exercise tolerance

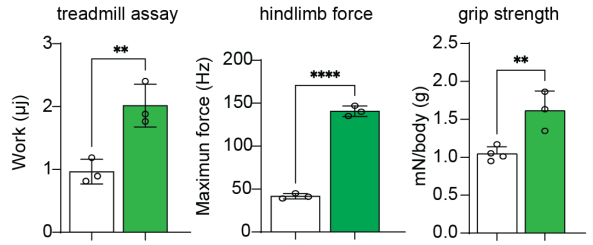


**C** glucose homeostasis

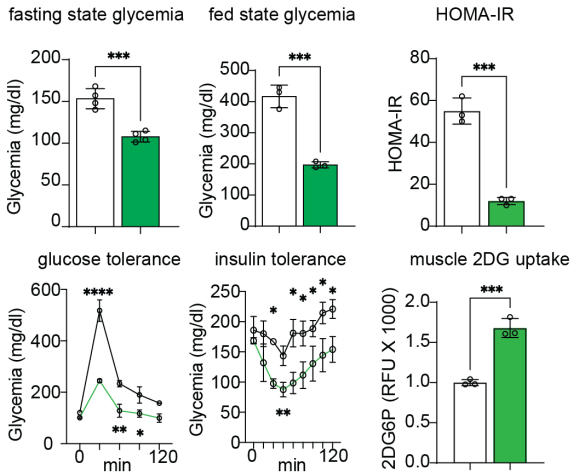


**D** insulin signaling pathway in muscle

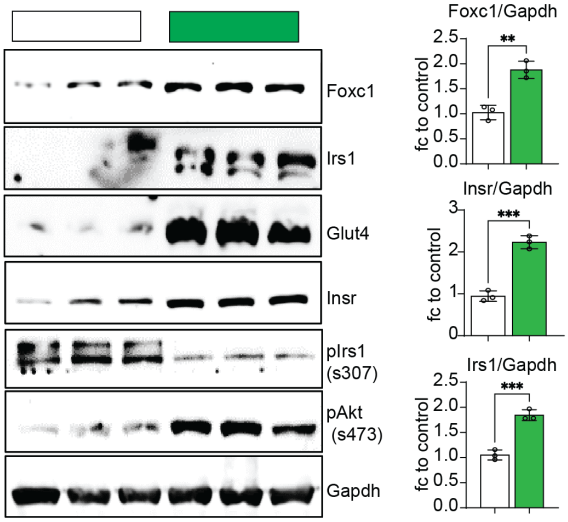


**E** Arid5a targets expression in muscle

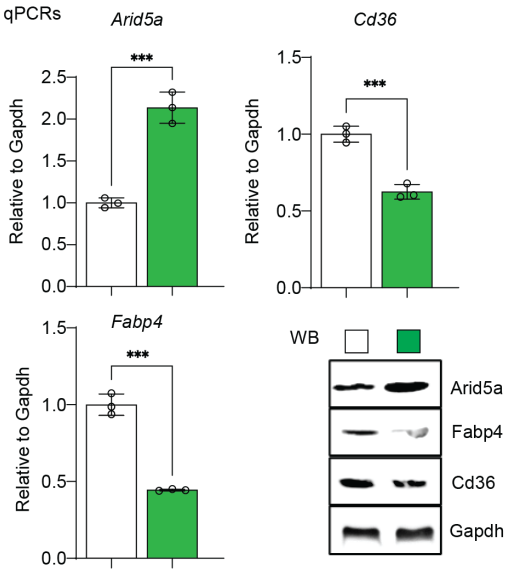


**F** in vivo sufficiency of muscle Foxc1 and Arid5a for protection against diet adverse effects

muscle from WT mice receiving AAV delivery together with high-fat diet onset MyoAAV-GFP MyoAAV-Foxc1 + MyoAAV-Arid5a

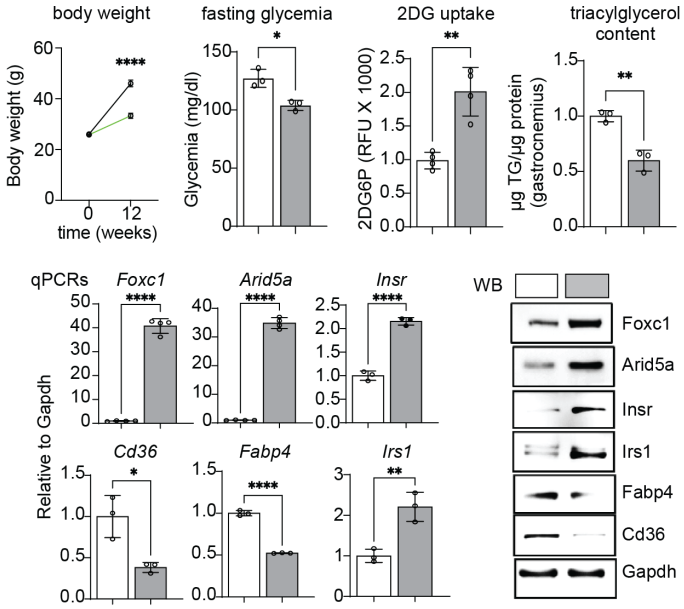

**Figure 5. The mutant GR protects muscle from insulin resistance and lipid accumulation with high-fat diet. (A)** Mutant male mice resisted weight gain significantly after a 12-week-long high-fat diet exposure, exhibiting a remarkable decrease in macroscopic fat accumulation in hindlimb muscles and significant improvements in lean and muscle masses. **(B)** Mutant obese mice showed improved exercise tolerance and force compared to obese controls. **(C)** Glucose homeostasis and muscle 2DG uptake was improved in mutant mice. **(D)** WB analysis of whole and phosphorylated proteins showed increased activation of Foxc1 and its targets in the insulin response pathway in mutant obese muscle compared to control obese muscle. **(E)** Arid5a was increased and its transactivation targets decreased in the mutant obese muscle. **(F)** Combination of in vivo muscle overexpression of both Foxc1 and Arid5a recapitulated the SNP effect on parameters of muscle insulin resistance and triacylglycerol accumulation, partially protecting the transduced mice from the adverse effects of high-fat diet. N=3-4/group; Welch's t-test (histograms), 2w ANOVA + Sidak (curves); *, $P<0.05$; **, $P<0.01$; ***, $P<0.001$; ****, $P<0.0001$.

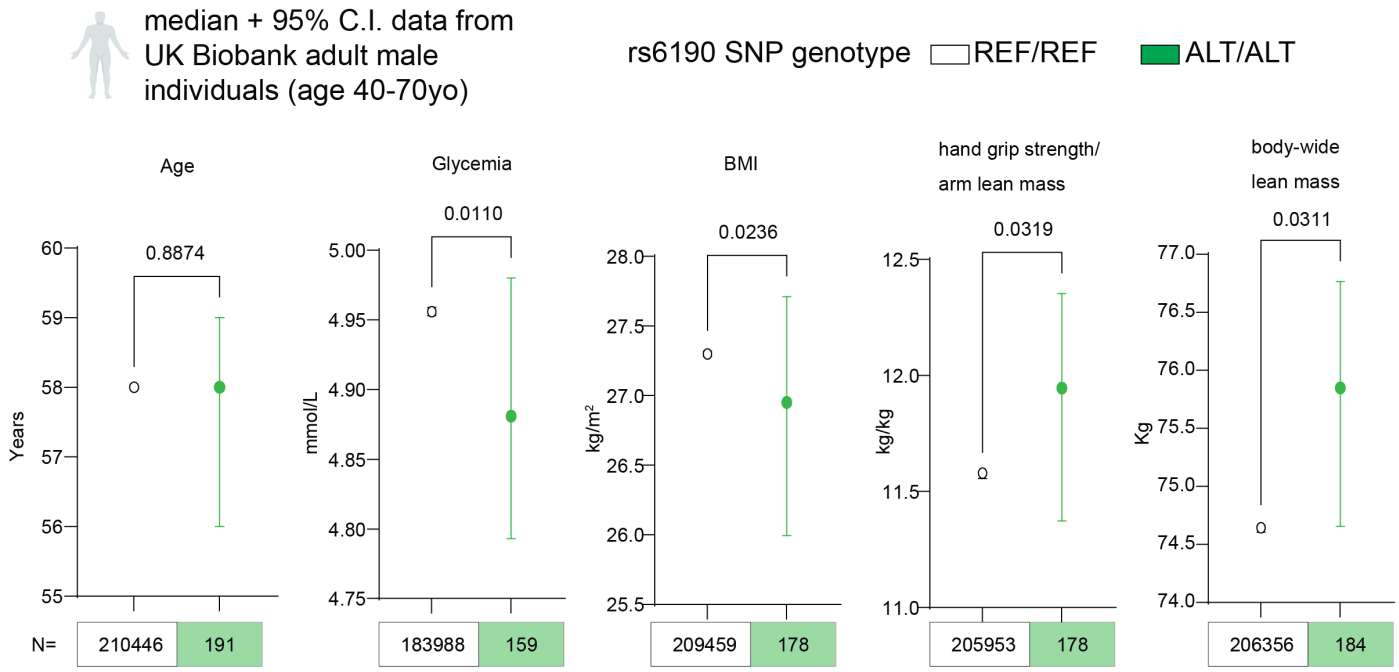


**Figure 6. Homozygosity for the rs6190 ALT allele correlates with improved median values of glycemia, BMI, grip strength and lean mass in the adult male UK Biobank population.** Cross-sectional analysis of UK biobank male cohort data showed that homozygous carriers of the rs6190 ALT allele (orthologous to the $GR^{R24K}$ allele in our transgenic mice) showed improved trends in glycemia, lean mass, BMI and grip strength compared to non-carriers, in the absence of age differences. Mann Whitney U-test. Regression analyses and cross-sectional comparisons including heterozygous carriers are presented in Tables 1 and 2.

## REFERENCES


[1] Hoffman, E.L., VonWald, T., Hansen, K., 2015. The metabolic syndrome. S D Med Spec No:24-28.

[2] Baron, A.D., Brechtel, G., Wallace, P., Edelman, S.V., 1988. Rates and tissue sites of non-insulin- and insulin-mediated glucose uptake in humans. Am J Physiol 255(6 Pt 1):E769-774.

[3] Haines, M.S., Leong, A., Porneala, B.C., Meigs, J.B., Miller, K.K., 2022. Association between muscle mass and diabetes prevalence independent of body fat distribution in adults under 50 years old. Nutr Diabetes 12(1):29.

[4] Standl, E., Schnell, O., McGuire, D.K., 2016. Heart Failure Considerations of Antihyperglycemic Medications for Type 2 Diabetes. Circ Res 118(11):1830-1843.

[5] Wijnen, M., Duschek, E.J.J., Boom, H., van Vliet, M., 2022. The effects of antidiabetic agents on heart failure. Neth Heart J 30(2):65-75.

[6] Khan, M.A.B., Hashim, M.J., King, J.K., Govender, R.D., Mustafa, H., Al Kaabi, J., 2020. Epidemiology of Type 2 Diabetes - Global Burden of Disease and Forecasted Trends. J Epidemiol Glob Health 10(1):107-111.

[7] Chadt, A., Scherneck, S., Joost, H.G., Al-Hasani, H., 2000. Molecular links between Obesity and Diabetes: "Diabesity". In: Feingold, K.R., Anawalt, B., Blackman, M.R., Boyce, A., Chrousos, G., Corpas, E., et al., editors. Endotext: South Dartmouth (MA).

[8] Merz, K.E., Thurmond, D.C., 2020. Role of Skeletal Muscle in Insulin Resistance and Glucose Uptake. Compr Physiol 10(3):785-809.

[9] DeFronzo, R.A., Tripathy, D., 2009. Skeletal muscle insulin resistance is the primary defect in type 2 diabetes. Diabetes Care 32 Suppl 2(Suppl 2):S157-163.

[10] Heitzer, M.D., Wolf, I.M., Sanchez, E.R., Witchel, S.F., DeFranco, D.B., 2007. Glucocorticoid receptor physiology. Rev Endocr Metab Disord 8(4):321-330.

[11] Sacta, M.A., Chinenov, Y., Rogatsky, I., 2016. Glucocorticoid Signaling: An Update from a Genomic Perspective. Annu Rev Physiol 78:155-180.

[12] Kuo, T., Harris, C.A., Wang, J.C., 2013. Metabolic functions of glucocorticoid receptor in skeletal muscle. Mol Cell Endocrinol 380(1-2):79-88.

[13] Salamone, I.M., Quattrocelli, M., Barefield, D.Y., Page, P.G., Tahtah, I., Hadhazy, M., et al., 2022. Intermittent glucocorticoid treatment enhances skeletal muscle performance through sexually dimorphic mechanisms. J Clin Invest 132(6).

[14] Quattrocelli, M., Salamone, I.M., Page, P.G., Warner, J.L., Demonbreun, A.R., McNally, E.M., 2017. Intermittent Glucocorticoid Dosing Improves Muscle Repair and Function in Mice with Limb-Girdle Muscular Dystrophy. Am J Pathol 187(11):2520-2535.

[15] Quax, R.A., Manenschijn, L., Koper, J.W., Hazes, J.M., Lamberts, S.W., van Rossum, E.F., et al., 2013. Glucocorticoid sensitivity in health and disease. Nat Rev Endocrinol 9(11):670-686.

[16] Leventhal, S.M., Lim, D., Green, T.L., Cantrell, A.E., Cho, K., Greenhalgh, D.G., 2019. Uncovering a multitude of human glucocorticoid receptor variants: an expansive survey of a single gene. BMC Genet 20(1):16.

[17] Koper, J.W., van Rossum, E.F., van den Akker, E.L., 2014. Glucocorticoid receptor polymorphisms and haplotypes and their expression in health and disease. Steroids 92:62-73.

[18] Niu, N., Manickam, V., Kalari, K.R., Moon, I., Pelleymounter, L.L., Eckloff, B.W., et al., 2009. Human glucocorticoid receptor alpha gene (NR3C1) pharmacogenomics: gene resequencing and functional genomics. J Clin Endocrinol Metab 94(8):3072-3084.

[19] Huizenga, N.A., Koper, J.W., De Lange, P., Pols, H.A., Stolk, R.P., Burger, H., et al., 1998. A polymorphism in the glucocorticoid receptor gene may be associated with and increased sensitivity to glucocorticoids in vivo. J Clin Endocrinol Metab 83(1):144-151.

[20] van Rossum, E.F., Koper, J.W., van den Beld, A.W., Uitterlinden, A.G., Arp, P., Ester, W., et al., 2003. Identification of the BclI polymorphism in the glucocorticoid receptor gene: association with sensitivity to glucocorticoids in vivo and body mass index. Clin Endocrinol (Oxf) 59(5):585-592.

[21] Manenschijn, L., van den Akker, E.L., Lamberts, S.W., van Rossum, E.F., 2009. Clinical features associated with glucocorticoid receptor polymorphisms. An overview. Ann N Y Acad Sci 1179:179-198.

[22] van Rossum, E.F., Koper, J.W., Huizenga, N.A., Uitterlinden, A.G., Janssen, J.A., Brinkmann, A.O., et al., 2002. A polymorphism in the glucocorticoid receptor gene, which decreases sensitivity to glucocorticoids in vivo, is associated with low insulin and cholesterol levels. Diabetes 51(10):3128-3134.

[23] van den Akker, E.L., Russcher, H., van Rossum, E.F., Brinkmann, A.O., de Jong, F.H., Hokken, A., et al., 2006. Glucocorticoid receptor polymorphism affects transrepression but not transactivation. J Clin Endocrinol Metab 91(7):2800-2803.
[24] Koper, J.W., Stolk, R.P., de Lange, P., Huizenga, N.A., Molijn, G.J., Pols, H.A., et al., 1997. Lack of association between five polymorphisms in the human glucocorticoid receptor gene and glucocorticoid resistance. Hum Genet 99(5):663-668.
[25] van Rossum, E.F., Voorhoeve, P.G., te Velde, S.J., Koper, J.W., Delemarre-van de Waal, H.A., Kemper, H.C., et al., 2004. The ER22/23EK polymorphism in the glucocorticoid receptor gene is associated with a beneficial body composition and muscle strength in young adults. J Clin Endocrinol Metab 89(8):4004-4009.
[26] Gerlinger-Romero, F., Addinsall, A.B., Lovering, R.M., Foletta, V.C., van der Poel, C., Della-Gatta, P.A., et al., 2019. Non-invasive Assessment of Dorsiflexor Muscle Function in Mice. J Vis Exp(143).
[27] Matthews, D.R., Hosker, J.P., Rudenski, A.S., Naylor, B.A., Treacher, D.F., Turner, R.C., 1985. Homeostasis model assessment: insulin resistance and beta-cell function from fasting plasma glucose and insulin concentrations in man. Diabetologia 28(7):412-419.
[28] Ueyama, A., Sato, T., Yoshida, H., Magata, K., Koga, N., 2000. Nonradioisotope assay of glucose uptake activity in rat skeletal muscle using enzymatic measurement of 2-deoxyglucose 6-phosphate in vitro and in vivo. Biol Signals Recept 9(5):267-274.
[29] Karwi, Q.G., Wagg, C.S., Altamimi, T.R., Uddin, G.M., Ho, K.L., Darwesh, A.M., et al., 2020. Insulin directly stimulates mitochondrial glucose oxidation in the heart. Cardiovasc Diabetol 19(1):207.
[30] Shintaku, J., Guttridge, D.C., 2016. Analysis of Aerobic Respiration in Intact Skeletal Muscle Tissue by Microplate-Based Respirometry. Methods Mol Biol 1460:337-343.
[31] Kumar, R., Thompson, E.B., 2012. Folding of the glucocorticoid receptor N-terminal transactivation function: dynamics and regulation. Mol Cell Endocrinol 348(2):450-456.
[32] Baker, J.D., Ozsan, I., Rodriguez Ospina, S., Gulick, D., Blair, L.J., 2018. Hsp90 Heterocomplexes Regulate Steroid Hormone Receptors: From Stress Response to Psychiatric Disease. Int J Mol Sci 20(1).
[33] Reis, L.M., Maheshwari, M., Capasso, J., Atilla, H., Dudakova, L., Thompson, S., et al., 2023. Axenfeld-Rieger syndrome: more than meets the eye. J Med Genet 60(4):368-379.
[34] Motojima, M., Tanaka, M., Kume, T., 2022. Foxc1 and Foxc2 are indispensable for the maintenance of nephron and stromal progenitors in the developing kidney. J Cell Sci 135(19).
[35] Rouillard, A.D., Gundersen, G.W., Fernandez, N.F., Wang, Z., Monteiro, C.D., McDermott, M.G., et al., 2016. The harmonizome: a collection of processed datasets gathered to serve and mine knowledge about genes and proteins. Database (Oxford) 2016.
[36] Hilder, T.L., Tou, J.C., Grindeland, R.E., Wade, C.E., Graves, L.M., 2003. Phosphorylation of insulin receptor substrate-1 serine 307 correlates with JNK activity in atrophic skeletal muscle. FEBS Lett 553(1-2):63-67.
[37] Brozinick, J.T., Jr., Birnbaum, M.J., 1998. Insulin, but not contraction, activates Akt/PKB in isolated rat skeletal muscle. J Biol Chem 273(24):14679-14682.
[38] Tabebordbar, M., Lagerborg, K.A., Stanton, A., King, E.M., Ye, S., Tellez, L., et al., 2021. Directed evolution of a family of AAV capsid variants enabling potent muscle-directed gene delivery across species. Cell 184(19):4919-4938 e4922.
[39] Chalise, J.P., Hashimoto, S., Parajuli, G., Kang, S., Singh, S.K., Gemechu, Y., et al., 2019. Feedback regulation of Arid5a and Ppar-gamma2 maintains adipose tissue homeostasis. Proc Natl Acad Sci U S A 116(30):15128-15133.
[40] Szklarczyk, D., Kirsch, R., Koutrouli, M., Nastou, K., Mehryary, F., Hachilif, R., et al., 2023. The STRING database in 2023: protein-protein association networks and functional enrichment analyses for any sequenced genome of interest. Nucleic Acids Res 51(D1):D638-D646.
[41] Zhang, Y., Sun, Z.W., Iratni, R., Erdjument-Bromage, H., Tempst, P., Hampsey, M., et al., 1998. SAP30, a novel protein conserved between human and yeast, is a component of a histone deacetylase complex. Mol Cell 1(7):1021-1031.
[42] Thiebaud, D., Jacot, E., DeFronzo, R.A., Maeder, E., Jequier, E., Felber, J.P., 1982. The effect of graded doses of insulin on total glucose uptake, glucose oxidation, and glucose storage in man. Diabetes 31(11):957-963.
[43] Ferrannini, E., Simonson, D.C., Katz, L.D., Reichard, G., Jr., Bevilacqua, S., Barrett, E.J., et al., 1988. The disposal of an oral glucose load in patients with non-insulin-dependent diabetes. Metabolism 37(1):79-85.
[44] Mesinovic, J., Zengin, A., De Courten, B., Ebeling, P.R., Scott, D., 2019. Sarcopenia and type 2 diabetes mellitus: a bidirectional relationship. Diabetes Metab Syndr Obes 12:1057-1072.

[45] Warram, J.H., Martin, B.C., Krolewski, A.S., Soeldner, J.S., Kahn, C.R., 1990. Slow glucose removal rate and hyperinsulinemia precede the development of type II diabetes in the offspring of diabetic parents. Ann Intern Med 113(12):909-915.
[46] Haynes, R.C., Jr., 1962. Studies of an vitro effect of glucocorticoids on gluconeogenesis. Endocrinology 71:399-406.
[47] Fain, J.N., Kovacev, V.P., Scow, R.O., 1965. Effect of growth hormone and dexamethasone on lipolysis and metabolism in isolated fat cells of the rat. J Biol Chem 240(9):3522-3529.
[48] Overman, R.A., Yeh, J.Y., Deal, C.L., 2013. Prevalence of oral glucocorticoid usage in the United States: a general population perspective. Arthritis Care Res (Hoboken) 65(2):294-298.
[49] Arvidson, N.G., Gudbjornsson, B., Larsson, A., Hallgren, R., 1997. The timing of glucocorticoid administration in rheumatoid arthritis. Ann Rheum Dis 56(1):27-31.
[50] Quattrocelli, M., Wintzinger, M., Miz, K., Panta, M., Prabakaran, A.D., Barish, G.D., et al., 2022. Intermittent prednisone treatment in mice promotes exercise tolerance in obesity through adiponectin. J Exp Med 219(5).
[51] Quattrocelli, M., Wintzinger, M., Miz, K., Levine, D.C., Peek, C.B., Bass, J., et al., 2022. Muscle mitochondrial remodeling by intermittent glucocorticoid drugs requires an intact circadian clock and muscle PGC1alpha. Sci Adv 8(7):eabm1189.
[52] Caratti, G., Stifel, U., Caratti, B., Jamil, A.J.M., Chung, K.J., Kiehntopf, M., et al., 2023. Glucocorticoid activation of anti-inflammatory macrophages protects against insulin resistance. Nat Commun 14(1):2271.
[53] van Rossum, E.F., Feelders, R.A., van den Beld, A.W., Uitterlinden, A.G., Janssen, J.A., Ester, W., et al., 2004. Association of the ER22/23EK polymorphism in the glucocorticoid receptor gene with survival and C-reactive protein levels in elderly men. Am J Med 117(3):158-162.
[54] Russcher, H., Smit, P., van den Akker, E.L., van Rossum, E.F., Brinkmann, A.O., de Jong, F.H., et al., 2005. Two polymorphisms in the glucocorticoid receptor gene directly affect glucocorticoid-regulated gene expression. J Clin Endocrinol Metab 90(10):5804-5810.
[55] Brovkina, A.F., Sychev, D.A., Toropova, O.S., 2020. [Influence of CYP3A4, CYP3A5, and NR3C1 genes polymorphism on the effectiveness of glucocorticoid therapy in patients with endocrine ophthalmopathy]. Vestn Oftalmol 136(6. Vyp. 2):125-132.
[56] Russo, P., Tomino, C., Santoro, A., Prinzi, G., Proietti, S., Kisialiou, A., et al., 2019. FKBP5 rs4713916: A Potential Genetic Predictor of Interindividual Different Response to Inhaled Corticosteroids in Patients with Chronic Obstructive Pulmonary Disease in a Real-Life Setting. Int J Mol Sci 20(8).
[57] El-Fayoumi, R., Hagras, M., Abozenadaha, A., Bawazir, W., Shinawi, T., 2018. Association Between NR3C1 Gene Polymorphisms and Toxicity Induced by Glucocorticoids Therapy in Saudi Children with Acute Lymphoblastic Leukemia. Asian Pac J Cancer Prev 19(5):1415-1423.
[58] Roerink, S.H., Wagenmakers, M.A., Smit, J.W., van Rossum, E.F., Netea-Maier, R.T., Plantinga, T.S., et al., 2016. Glucocorticoid receptor polymorphisms modulate cardiometabolic risk factors in patients in long-term remission of Cushing's syndrome. Endocrine 53(1):63-70.
[59] Quax, R.A., Koper, J.W., Huisman, A.M., Weel, A., Hazes, J.M., Lamberts, S.W., et al., 2015. Polymorphisms in the glucocorticoid receptor gene and in the glucocorticoid-induced transcript 1 gene are associated with disease activity and response to glucocorticoid bridging therapy in rheumatoid arthritis. Rheumatol Int 35(8):1325-1333.
[60] Bouma, E.M., Riese, H., Nolte, I.M., Oosterom, E., Verhulst, F.C., Ormel, J., et al., 2011. No associations between single nucleotide polymorphisms in corticoid receptor genes and heart rate and cortisol responses to a standardized social stress test in adolescents: the TRAILS study. Behav Genet 41(2):253-261.
[61] Fraulob, J.C., Ogg-Diamantino, R., Fernandes-Santos, C., Aguila, M.B., Mandarim-de-Lacerda, C.A., 2010. A Mouse Model of Metabolic Syndrome: Insulin Resistance, Fatty Liver and Non-Alcoholic Fatty Pancreas Disease (NAFPD) in C57BL/6 Mice Fed a High Fat Diet. J Clin Biochem Nutr 46(3):212-223.
[62] Emerald, B.S., Chng, K., Masuda, S., Sloboda, D.M., Vickers, M.H., Kambadur, R., et al., 2011. Gene expression profiling in the Cynomolgus macaque Macaca fascicularis shows variation within the normal birth range. BMC Genomics 12:509.
[63] Schmittgen, T.D., Livak, K.J., 2008. Analyzing real-time PCR data by the comparative C(T) method. Nat Protoc 3(6):1101-1108.
[64] Yamamoto, N., Yamashita, Y., Yoshioka, Y., Nishiumi, S., Ashida, H., 2016. Rapid Preparation of a Plasma Membrane Fraction: Western Blot Detection of Translocated Glucose Transporter 4 from Plasma Membrane of Muscle and Adipose Cells and Tissues. Current Protocols in Protein Science 85(1):29.18.21-29.18.12.

[65] Schneider, C.A., Rasband, W.S., Eliceiri, K.W., 2012. NIH Image to ImageJ: 25 years of image analysis. Nat Methods 9(7):671-675.
[66] Durumutla, H.B., Villa, C., Panta, M., Wintzinger, M., Pragasam, A.D.P., Miz, K., et al., 2023. Comprehensive Analyses of Muscle Function, Lean and Muscle Mass, and Myofiber Typing in Mice. Bio Protoc 13(4):e4617.
[67] Castro, B., Kuang, S., 2017. Evaluation of Muscle Performance in Mice by Treadmill Exhaustion Test and Whole-limb Grip Strength Assay. Bio Protoc 7(8).
[68] Quattrocelli, M., Zelikovich, A.S., Jiang, Z., Peek, C.B., Demonbreun, A.R., Kuntz, N.L., et al., 2019. Pulsed glucocorticoids enhance dystrophic muscle performance through epigenetic-metabolic reprogramming. JCI Insight 4(24).
[69] Burkholder, T.J., Fingado, B., Baron, S., Lieber, R.L., 1994. Relationship between muscle fiber types and sizes and muscle architectural properties in the mouse hindlimb. J Morphol 221(2):177-190.
[70] Mina, A.I., LeClair, R.A., LeClair, K.B., Cohen, D.E., Lantier, L., Banks, A.S., 2018. CalR: A Web-Based Analysis Tool for Indirect Calorimetry Experiments. Cell Metab 28(4):656-666 e651.
[71] Tschop, M.H., Speakman, J.R., Arch, J.R., Auwerx, J., Bruning, J.C., Chan, L., et al., 2011. A guide to analysis of mouse energy metabolism. Nat Methods 9(1):57-63.
[72] Schefer, V., Talan, M.I., 1996. Oxygen consumption in adult and AGED C57BL/6J mice during acute treadmill exercise of different intensity. Exp Gerontol 31(3):387-392.